Recent Progress in Electromagnetic Interference Shielding Performance of Porous Polymer Nanocomposites—A Review

Avinash R. Pai [1,2], **Nizam Puthiyaveettil Azeez** [3], **Binumol Thankan** [3], **Nandakumar Gopakumar** [4], **Maciej Jaroszewski** [5,*], **Claudio Paoloni** [2], **Nandakumar Kalarikkal** [1] and **Sabu Thomas** [1,3,6,*]

1 International and Inter University Centre for Nanoscience and Nanotechnology (IIUCNN), Mahatma Gandhi University, Kottayam 686560, India; avinashrpai@gmail.com (A.R.P.); nkkalarikkal@mgu.ac.in (N.K.)
2 Engineering Department, Lancaster University, Lancaster LA1 4YW, UK; c.paoloni@lancaster.ac.uk
3 School of Chemical Sciences, Mahatma Gandhi University, Kottayam 686560, India; nizam000@gmail.com (N.P.A.); binumoltanunivas999@gmail.com (B.T.)
4 Amrita School of Arts and Sciences, Amrita Viswa Vidyapeetham, Amritapuri 690525, India; nandakumarg705@gmail.com
5 Faculty of Electrical Engineering, Wroclaw University of Science and Technology, 50-370 Wroclaw, Poland
6 School of Energy Materials, Mahatma Gandhi University, Kottayam 686560, India
* Correspondence: maciej.jaroszewski@pwr.edu.pl (M.J.); sabuthomas@mgu.ac.in (S.T.)

Abstract: The urge to develop high-speed data transfer technologies for futuristic electronic and communication devices has led to more incidents of serious electromagnetic interference and pollution. Over the past decade, there has been burgeoning research interests to design and fabricate high-performance porous EM shields to tackle this undesired phenomenon. Polymer nanocomposite foams and aerogels offer robust, flexible and lightweight architectures with tunable microwave absorption properties and are foreseen as potential candidates to mitigate electromagnetic pollution. This review covers various strategies adopted to fabricate 3D porous nanocomposites using conductive nanoinclusions with suitable polymer matrices, such as elastomers, thermoplastics, bioplastics, conducting polymers, polyurethanes, polyimides and nanocellulose. Special emphasis has been placed on novel 2D materials such as MXenes, that are envisaged to be the future of microwave-absorbing materials for next-generation electronic devices. Strategies to achieve an ultra-low percolation threshold using environmentally benign and facile processing techniques have been discussed in detail.

Keywords: polymer nanocomposites; porous; foams; aerogels; EMI shielding; microwave absorption

1. Introduction

Electromagnetic (EM) pollution is a severe concern that needs to be addressed by microwave engineers and material scientists working on next-generation electronic devices functioning at a higher bandwidth of the microwave region. With the quest towards miniaturization of electronic gadgets, there has been a tremendous impact on the modern technology and operating speeds of these devices. This miniaturization of electronic components eventually paved the way for undesirable mixing of electronic impulses, which is termed electromagnetic interference (EMI) and is envisaged to have detrimental effects on the overall performance and lifespan of high-frequency devices. There is no confirmed evidence of health risk from EM radiation generated by mobile phones. However, particularly in work environment the EM pollution could be increase the body temperature or affect the functioning of e.g. pacemakers [1–3]. Most of the medical implant devices such as hearing aids, insulin pumps and cardiac pacemakers also work on EM signals and could result in malfunctioning upon exposure to alternating EM fields [4]. Military communication systems mostly rely on distinct GHz frequencies and are also vulnerable to the problem of EMI, which is a serious national threat to the defense and allied sectors. Conventionally, thin metallic foils were used to suppress EM radiation, but they scatter the incident

signals due to the mismatch of impedance between the incoming EM wave and the metal surface. The presence of free valence electrons in metals paves the way to interact with the microwave radiation and eventually reduces the intensity of the incident waves. However, this creates further EM pollution and is not considered as an effective way to prevent EMI. Numerous demerits viz. poor corrosion resistance, low flexibility and high density further limits their use as EMI shields. Hence, to mitigate this undesired phenomenon, researchers are working in an interdisciplinary fashion to devise high-performance EMI shielding materials that primarily absorb EM radiation. Therefore, EMI shielding of devices using conductive, robust, flexible and lightweight polymer nanocomposite foams and aerogels have attracted researchers in the past few decades [5].

The main criterion for designing polymeric EMI shields with high shielding effectiveness is by inclusion of electric and magnetic dipoles into the system [6]. EM waves, being a synchronous propagation of mutually perpendicular electric and magnetic fields, can interact with the electric and magnetic dipoles, hence reflecting or absorbing the incident EM waves. Owing to the ease of processability, superior mechanical properties, flexibility and tailored functional properties, polymer nanocomposites are potential candidates for designing efficient EMI shielding materials [7–16]. Effective EMI shields with a predominant absorption mechanism can be formulated by incorporating magnetic and dielectric nanostructures, which will in turn enhance the complex permittivity and permeability of the shields [17–19]. Numerous polymer nanocomposites with judicious combinations of conducting fillers, such as 1D fillers (carbon nanofibers [20–22], carbon nanotubes [23–31], metal nanowires [32–35]), 2D fillers (graphene [36–39], reduced graphene oxide [40–43], hBN [44–47], MoS_2 [48–51], MXene [52–56]), magnetic fillers (Fe_3O_4 [57–59], Fe_2O_3 [60,61], nickel ferrite [62,63]) and dielectric fillers ($BaTiO_3$ [64], barium strontium titanate [65,66] and TiO_2 [67,68]) have been extensively studied for designing efficient EMI shielding materials that can overcome the drawbacks of conventionally used metallic shields. In addition, conducting polymers such as polyaniline [69–72], polypyrrole [73–76], PEDOT:PSS [77–79] and polythiophene [80–82] have also been extensively utilized to shield EM waves. They offer tunable electrical conductivities but have poor processability and film-forming capabilities, which hinders their viability as robust shields. Hence, conducting polymers are incorporated as fillers or blended with commodity polymers to fabricate EM shields for commercial applications. However, for designing thinner and lighter shields with a very low percolation threshold of nanofillers, many pitfalls in existing EMI shielding materials' research should be addressed [83].

It is well-known that the electrical conductivity is of paramount importance and directly governs the EMI shielding performance of any polymer nanocomposite shield [84]. For any shield to absorb EM radiation, it is also highly desired to tune the dielectric constant to be very close to that of air. The shields mostly reflect back signals due to the mismatch of impedance between the propagating signal medium and the shield surface. Hence, foaming of polymer nanocomposites is regarded as an impending strategy to fabricate lightweight and high-performance EMI absorbers. The relative volume of air entrapped within the porous framework of foams and aerogels is indeed very high, which facilitates better impedance matching. The porous network of conducting nanofillers within the foams also provides multiple filler–polymer interfaces that will result in multiple internal scatterings or reflections. This will eventually lead to microwave absorption and heat dissipation. Aerogels are yet another class of porous materials, like polymer foams, with excellent physicochemical attributes, such as ultra-low density (0.003–0.500 g/cm^3) and higher porosities (80–99.8%), that are useful for high-end technological applications such as thermal insulation, oil recovery and catalysis [85–87]. However, in the context of EMI shielding applications, polymer nanocomposite foams and aerogels possess many similarities in the mechanism of shielding due to the presence of a well-interconnected porous network, which is available to scatter EM radiation. Moreover, the key challenge for designing high-performance polymer nanocomposite foams and aerogels is proper selection of the polymer matrix and nanofiller system. The wettability, degree of dispersion and nanofiller–polymer

interaction is of paramount importance to achieve good electrical conductivity and high EMI shielding efficacy in polymer nanocomposite shields. Henceforth, in this review, various strategies adopted to fabricate polymer nanocomposite foams and aerogels for superior microwave absorption and high EMI shielding performance have been discussed in detail. Methodologies adopted to achieve an ultra-low percolation threshold at minimal nanofiller concentrations are also discussed in detail. In the last decade, a significant amount of work has been published in the area of EMI shielding material, especially focused on designing porous structures such as foam and aerogels. Figure 1 shows the number of publications reported during the last decade (2011–2020) in ScienceDirect and Web of Science databases, with keywords such as electromagnetic interference shielding, porous, foam and aerogels, which clearly depicts the rising interest among the research community to fabricate porous microwave absorbers for next-generation technologies.
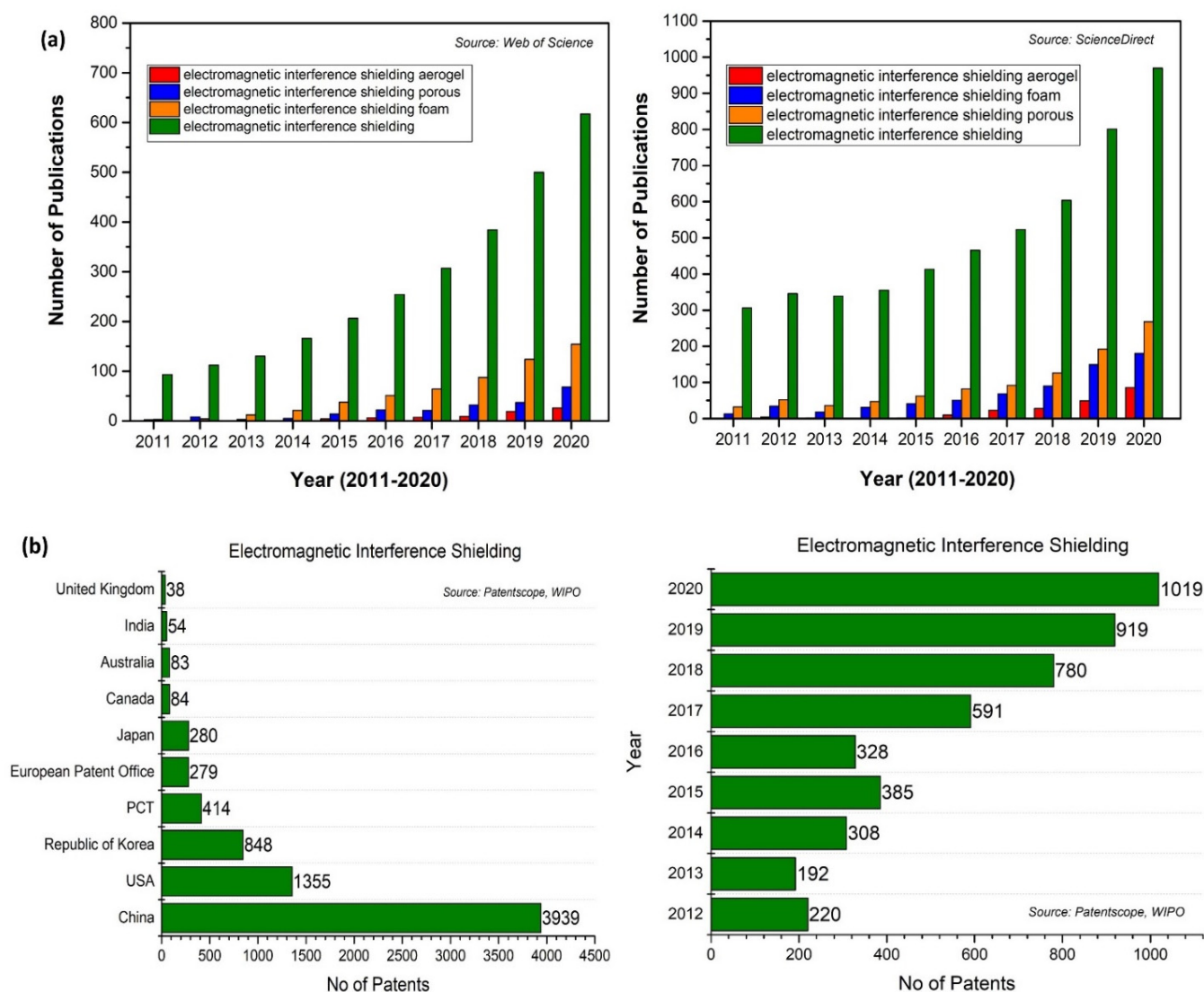
Figure 1. (**a**) Year-wise number of publications and (**b**) patents in the area of porous EMI shielding materials (foams and aerogels) over the last decade (2011–2021).

2. Terminologies in EMI Shielding

Firstly, there are two major parameters that need to be quantified for characterizing the efficiency of any electromagnetic shield material. The first is the shielding effectiveness (SE) and the second is the reflectivity (R) of the shield. The former corresponds to the measure of power which is transmitted through the shield material (P_T) to the incident power (P_I), and

the latter corresponds to the power reflected back from the shield (P_R) to the incident power. In general, the shielding effectiveness is expressed in terms of reductions in the magnitude of the incoming power when power is transmitted through the shield. In general, the total shielding efficiency of a shield is expressed on a logarithmic scale, as shown below [88]:

$$\text{SE}_T(\text{dB}) = \text{SE}_A + \text{SE}_R + \text{SE}_M = 10\log_{10}\left(\frac{P_T}{P_I}\right) = 20\log_{10}\left(\frac{E_T}{E_I}\right) = 20\log_{10}\left(\frac{H_T}{H_I}\right) \quad (1)$$

where P_I (E_I or H_I) and P_T (E_T or H_T) are the power (electric/magnetic field intensities) of incoming and transmitted EM waves, respectively. The aforementioned equation clearly suggests that the total electromagnetic shielding efficiency of a material depends on the sum of the three different mechanisms, viz. shielding by absorption (SE_A), reflection (SE_R) and multiple internal reflections (SE_M). Figure 2 depicts a schematic illustration of the different electromagnetic shielding mechanisms.
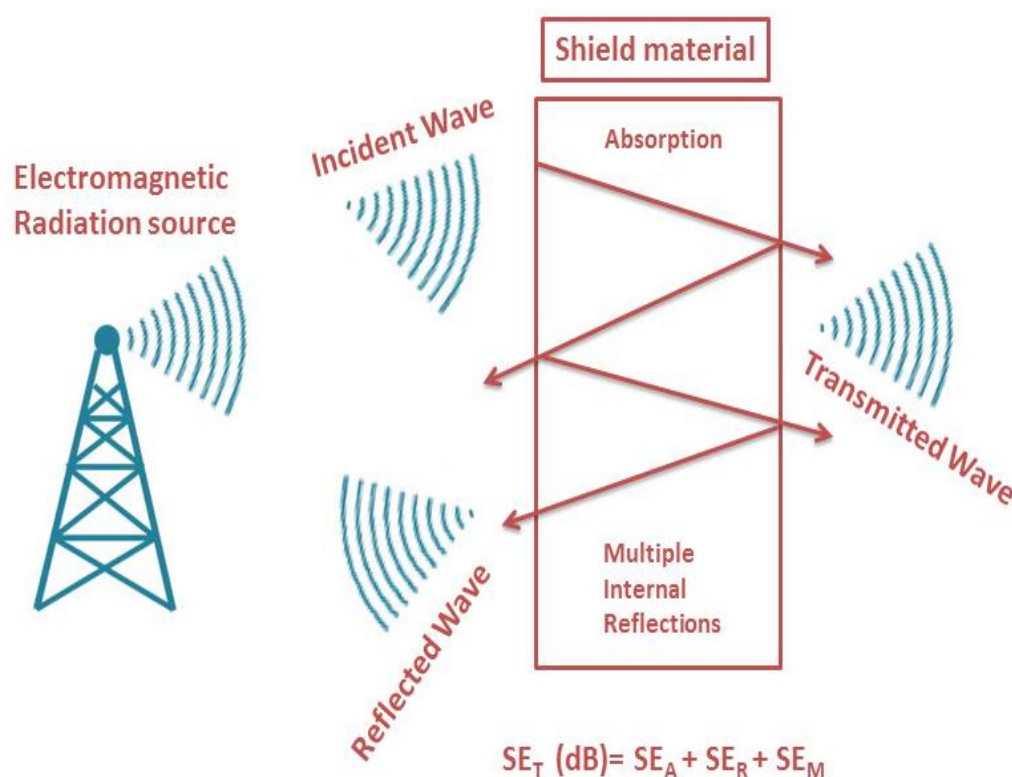
Figure 2. Plausible EMI shielding mechanisms associated with a shield material.

The incident EM wave is either reflected back to the surrounding areas or is transmitted through the material, or will be absorbed inside the material. However, it is highly desirable to fabricate materials which have high conductivity and low reflectivity. For instance, metals are used as conventional EMI shielding materials with high SE values, but at the same time, most of the incoming EM wave is reflected back to the adjacent electronic circuits. This leads to further EM interference, and hence there is a strong need to develop microwave-absorbing materials which have high SE values and low reflectivity in the noted frequency region. For such materials, they must exhibit high conductivity (for high SE values) and a low dielectric constant (for low reflectivity).

2.1. Shielding by Absorption (SE_A)

When an EM wave passes through any medium, its intensity becomes exponentially reduced. The critical thickness at which the EM field strength reduces to $1/e$ of the incident field is known as the skin depth (δ). This decay occurs as currents induced in the material

produce ohmic losses, which also heats up the material. The absorption losses within a shield can be expressed by the following equation [89]:

$$SE_A = -20\frac{t}{\delta}\,\log_{10} e = -8.68\left(\frac{t}{\delta}\right) = -8.68\,t\left(\frac{\sigma_T\mu_r\omega}{2}\right)^{\frac{1}{2}} \tag{2}$$

where t is the thickness of the shield in inches, δ is the skin depth and f is the frequency in Hz. It is also evident from the above expression that SE_A is directly proportional to the square root of the product of permeability (μ_r) and conductivity (σ_T). In addition, the SE_A of a given material also increases with increasing frequency. The skin depth (δ) of a shield can be expressed as the following equation [89]:

$$\delta = \sqrt{\frac{2}{f\mu\sigma}} = -8.68 \times \frac{t}{SE_A} \tag{3}$$

where t is the thickness of the shield, f is the frequency and σ is the electrical conductivity, respectively. However, it is evident that the skin depth of the shielding material has a direct relation with the thickness of the shield. In such case, two situations are possible.

When (t << δ): The material is called electrically thin when the thickness of the shield is less than the skin depth, and this generally occurs at lower frequencies. In this situation, the shielding due to absorption can be ignored and attenuation occurs mostly through the reflection mechanism. Then, the total shielding becomes independent of frequency and can be expressed in terms of free space impedance, as follows [89]:

$$SE\,(dB) = -20\log_{10}\left(1 + \frac{Z_0}{2}\,t\sigma_T\right) \tag{4}$$

where Z_0 is the impedance of the free space (=377 Ω).

When (t >> δ): The material is called electrically thick when the skin depth is much lower compared to the thickness of the shield. Here, the total SE can be calculated after making a good conductor approximation.

2.2. Shielding by Reflection (SE$_R$)

The reflection losses of a shield material under far-field conditions can be expressed as follows [89]:

$$SE_R(dB) = -10\,\log_{10}\left(\frac{\sigma_T}{16\,\omega\varepsilon_0\mu_r}\right) \tag{5}$$

where σ_T is the total conductivity, μ_r is the relative permeability and f is the frequency in Hz. The above equation shows that reflection losses are a function of the ratio of conductivity and permeability, i.e., (σ_T/μ_r). In addition, for a shield material with constant σ_T and μ_r, SE_R decreases with increasing frequency.

2.3. Shielding Due to Multiple Internal Reflections (SE$_M$)

When the thickness of the shield is low, the incident EM waves are reflected between the first and second boundaries. The shielding effectiveness due to multiple internal reflections, SE_M, is expressed as the following equation [89]:

$$SE_M = 20\log_{10}\left(1 - e^{-2t/\delta}\right) = 20\log_{10}\left[1 - 10^{\frac{-SE_A}{10}}\right] \tag{6}$$

From the above equation, it is clear that SE_M is directly related to absorption losses (SE_A). This loss is of more importance in foamed polymer nanocomposite materials, where air is present in the pores and hence reduces the dielectric constant of the material (dielectric constant of air = 1). As the dielectric constant decreases, the reflection losses will be minimal, and hence the shielding mechanism will be mostly governed by the absorption mechanism.

SE_M can be neglected when the thickness of the shield is high, then the SE_A value will be high, and by the time the EM waves reach the second boundary, its amplitude becomes negligible. In addition, if $SE_A \geq 10$ dB, SE_M can be neglected [89]. SE_M is usually important in cases of thin conductors when used at lower frequencies (in the KHz region). However, for absorbing shields in the high-frequency region (GHz region), if $SE_A \geq 10$ dB, SE_{MR} can be considered negligible.

The ability of any shield material to attenuate EM waves is termed as EMI shielding effectiveness (EMI SE), and is usually expressed in terms of decibels (dB). It can also be expressed in terms of percentage (%), which can be calculated with the following equation [90]:

$$\text{Shielding efficiency } (\%) = \left(\frac{1}{10^{\frac{SE}{10}}} \right) \times 100 \tag{7}$$

3. Reflection Loss (R_L) and Microwave Absorption

As per the transmission line theory, when an electromagnetic wave of fixed-frequency impinges perpendicularly on the surface of a single-layer absorbing material, the power reflection of the material can be calculated with the reflection loss coefficient, R_L (dB), given be the following equation [91]:

$$R_L(\text{dB}) = 20 \log \left| \frac{Z_{in} - Z_0}{Z_{in} - Z_0} \right| \tag{8}$$

$$Z_{in} = Z_0 \sqrt{\frac{\mu_r}{\varepsilon_r}} \tanh \left[j \left(\frac{2\pi f d}{c} \right) \sqrt{\mu_r \varepsilon_r} \right] \tag{9}$$

where $Z_0 \approx 377\ \Omega$, i.e., free space impedance, μ_r = complex permeability ($\mu_r = \mu' - j\mu''$), ε_r = complex permittivity ($\varepsilon_r = \varepsilon' - j\varepsilon''$), f = frequency, d = thickness of the material and c = speed of light. The percentage of microwave absorption and reflection loss, R_L, is governed by the following equation [92]:

$$\text{Microwave Absorption } (\%) = 100 - \left[10^{\left(\frac{R_L}{10} \right)} \times 100 \right] \tag{10}$$

The absorption efficacy of any EM absorber depends on the frequency of the EM wave, the thickness of the shield and the relative complex permeability and permittivity of the material. Another factor for enhanced EM absorption is better impedance matching. The condition for impedance matching is given by $Z_{in} = Z_0$, which means that the impedance at the shield surface should be made close to that of air so as to facilitate the passage of EM waves into the shield [93]. This can be made possible by introducing porosity and also fine-tuning the material properties such as permeability and permittivity. The R_L value is usually negative, and the larger the absolute value of R_L, the smaller the energy of the electromagnetic wave reflected by the material surface. This indicates that the majority of the EM energy is being absorbed and the material has better absorption efficiency. Table 1 presents a comparison between shielding effectiveness (dB) with shielding efficiency (%), and reflection loss (R_L) with microwave absorption. For instance, -10 dB shielding effectiveness corresponds to 90% attenuation of incident electromagnetic radiation. Similarly, a -20 dB EMI SE represents 99% blockage. Whereas an R_L value less than -10, -20 or -30 dB infers that more than 90%, 99% or 99.9% of the incident EM energy is absorbed. Usually, the bandwidth with R_L values less than -10 dB is considered as an effective electromagnetic absorption bandwidth (EAB) [94]. In practice, excellent microwave absorber materials should showcase an R_L value less than -10 dB within a broad frequency bandwidth at very low thickness. For commercial applications, a minimum of -20 dB shielding and R_L values lower than -10 dB over a wide range of bandwidth with minimal thickness is considered as an effective EMI shielding material.

Table 1. The correlation between the EMI shielding effectiveness value (dB) with shielding efficiency (%) and the reflection loss (R_L) value with microwave absorption (%). Reprinted/adapted with permission from Ref [90]. Copyright 2016, The American Association for the Advancement of Science.

EMI Shielding Effectiveness (dB)	Shielding Efficiency (%)	Reflection Loss (R_L) (dB)	Microwave Absorption (%)
0	0	0	0
−10	90	−10	90
−20	99	−20	99
−30	99.9	−30	99.9
−40	99.99	−40	99.99
−50	99.999	−50	99.999
−60	99.9999	−60	99.9999
−70	99.99999	−70	99.99999
−80	99.999999	−80	99.999999
−90	99.9999999	−90	99.9999999
−92	99.99999994	−92	99.99999994

4. Tuning Microwave Absorption for Superior EMI Shielding in Porous Materials

For any EMI shielding material to absorb excess EM radiation impinging on its surface, one should keep the dielectric constant equal to one or close to that of air. The reflection of EM radiation is primarily due to the impedance mismatch between the wave impedances of the signal propagating in air and those of the absorber material. A facile approach for this impedance matching is fabricating porous architectures of conductive polymer nanocomposites. The relative volume of air in these porous polymer nanocomposites is indeed very high, and thus facilitates better impedance matching at the shield/air interface. Nevertheless, the presence of air bubbles in the cells can reflect and scatter EM radiation and make it difficult to escape from the porous structure, and it eventually becomes absorbed and transferred as heat energy, as shown in Figure 3. The EMI SE value of these porous nanocomposites is mostly absorption-dominant due to this phenomenon. In addition, porous structures create multiple filler–polymer interfaces, where large amounts of charges would accumulate, thereby increasing the interfacial/space charge polarization and thus the EM attenuating capacity [95].
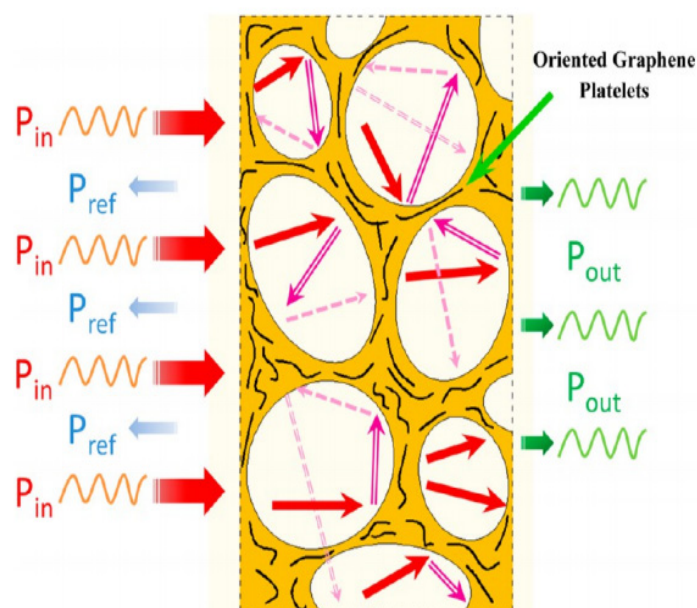
Figure 3. Schematic representation of microwave propagation and scattering across PEI/graphene nanocomposite foam. Reproduced with permission from [95]. Copyright 2013, American Chemical Society.

In general, porous materials are usually considered to be composites that are composed of solid and air components, where the Maxwell Garnett (MG) theory is an emblematic mechanism for understanding the variation of the effective permittivity. As per the MG theory, the effective permittivity in any porous material can be expressed as in the equation below [96]:

$$\varepsilon_{\text{eff}}^{\text{MG}} = \varepsilon_1 \left[\frac{(\varepsilon_2 + 2\varepsilon_1) + 2f(\varepsilon_2 - \varepsilon_1)}{(\varepsilon_2 + 2\varepsilon_1) - f(\varepsilon_2 + \varepsilon_1)} \right] \tag{11}$$

where ε_1 = permittivity of the solid component, ε_2 = permittivity of air and f = volume fraction of air. The permittivity of air is 1, and the solid component possesses a value higher than 1. From the above equation, one can deduce that the effective permittivity decreases with the increasing pore volume or void content. This will now facilitate towards better impedance matching and also promote incoming EM waves to enter into the absorber more easily. The presence of a porous architecture will therefore reduce complex permittivity. In general, EM attenuation capacity and good impedance matching are the fundamental design principles for high-performance microwave absorption. The characteristic input impedance can also be expressed in terms of relative complex permittivity (ε_r) and complex permeability (μ_r), as follows [97]:

$$Z_{\text{in}} = \sqrt{\frac{\mu_0}{\varepsilon_0}} \sqrt{\frac{\mu_r}{\varepsilon_r}} \tag{12}$$

where ε_0 and μ_0 are the permittivity and permeability of the vacuum. It is well-known that ε_r is usually larger than μ_r for any absorber material. Therefore, if the value of ε_r decreases, it will help to bring the Z_{in}/Z_0 value close to 1 and result in better impedance matching and enhanced microwave absorption.

The attenuation constant (α) is another parameter that determines the extent of microwave absorption performance. It can be expressed in terms of the dielectric and magnetic losses in an absorber using the following equation [97]:

$$\alpha = \frac{\sqrt{2}\pi f}{c} \sqrt{\mu'' \, \varepsilon'' - \mu'\epsilon' + \sqrt{(\mu''\epsilon'' - \mu'\epsilon')^2 + (\mu'\varepsilon'' + \mu''\varepsilon')^2}} \tag{13}$$

where f = frequency of electromagnetic wave propagation and c = velocity of light.

5. Solid vs.Porous EMI Shielding Materials

Electromagnetic shielding is directly correlated with the electrical properties of the nanocomposites. Several conducting nanoinclusions have been incorporated into polymer matrices, such as carbon nanotubes (CNTs), carbon nanofibers (CNFs), graphene, MXenes, magnetic NPs and ferrites, to fabricate electrically conductive polymer nanocomposites for EMI shielding and microwave absorption. The formation of a long-order interconnectivity of these nanofillers within the polymer matrix is of paramount importance to achieve the desired electrical conductivity and EMI shielding performance. In polymer nanocomposites, at a particular filler concentration there exists a critical point where a conductive filler network is formed, and the DC conductivity substantially increases. This point at which a nanocomposite becomes capable of conducting direct current is termed the percolation threshold. It is also well-established that below this percolation threshold, polymer composites act as mere insulators. As per the classical percolation theory, the relationship between the DC conductivity of a polymer/filler composite (σ_{dc}) and the volume fraction of the conducting filler (v_f) can be expressed as follows [98]:

$$\sigma_{\text{DC}} = \sigma_0 \left(\varnothing_f - \varnothing_c \right)^t \tag{14}$$

where σ_0 = conductivity of the filler, $\varnothing_f$ = volume fraction of the filler, $\varnothing_c$ = percolation threshold and t = critical exponent. This equation is valid for concentrations higher than the percolation threshold, i.e., $\varnothing_f > \varnothing_c$, and the critical exponent value depends on the

dimension and aspect ratio of the filler used in the system. In this region, the overall electrical conductivity is enhanced due to possible charge transport mechanisms, viz. conduction, tunneling or hopping. Conduction occurs when there is physical contact between neighboring fillers so that electrons can be transferred from one filler to another. However, for hopping and tunneling mechanisms, physical contact is not required for charge transport. Several strategies have been adopted to reduce the percolation threshold and achieve higher conductivity at extremely low filler concentrations. Fabricating porous polymer nanocomposites such as foams/aerogels is the mostly widely used technique to reduce the percolation threshold and enhance microwave absorption. A schematic representation of how the percolation threshold varies in foam and bulk polymer nanocomposites is depicted in Figure 4. Foamed polymer nanocomposites showcase similar electrical conductivity at lower volume fractions of filler ($\phi_{foam} < \phi_{Bulk}$) when compared to their bulk counterparts. In this context, Ling et al. [95] fabricated lightweight and porous polyetherimide (PEI)/graphene composite foams and examined the dependence of electrical conductivity and microwave absorption with solid nanocomposites. Interestingly, it was observed that via the foaming process, the percolation threshold significantly reduced from 0.21 to 0.18 vol.% for solid and foam nanocomposites, respectively. It is also worth mentioning that the percentage of microwave absorption in foam nanocomposites was found to be 8.1–14.4% more than in the solid shields [95].
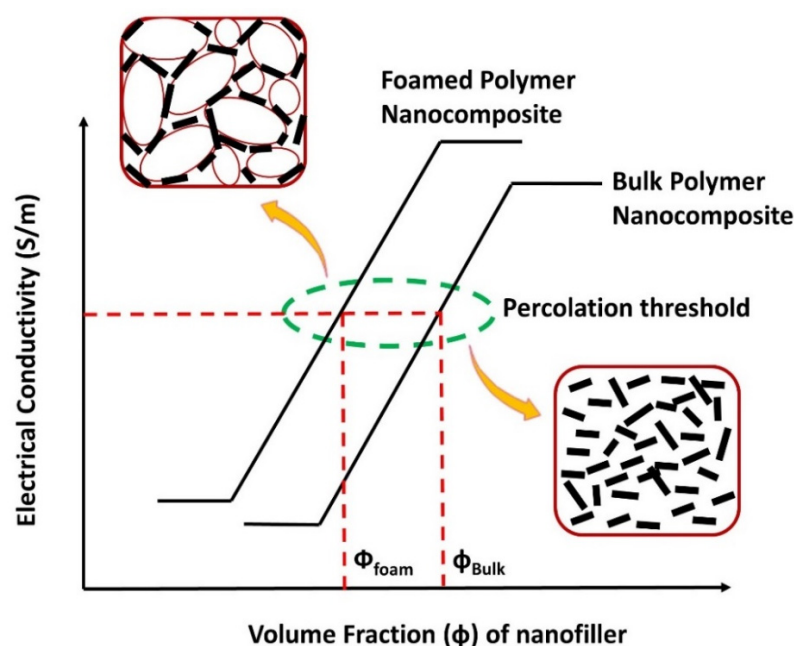
Figure 4. Schematic comparison of percolation behavior in bulk and porous polymer nanocomposites.

Hamidinejad et al. [99] performed extensive studies to understand the effect of foaming on the electrical conductivity and EMI shielding performance of HDPE-graphene nanoplatelet (GnP) composite foams. These composite foams were fabricated by physical foaming using the injection molding process. The degree of foaming greatly affected the electrical conductivity of these nanocomposites. The percolation threshold drastically decreased from 19 to 9.1 vol.% GnP at a 7% degree of foaming and due to the volume exclusion effect induced by the gas phase. In addition, a maximum EMI SE value of 31.6 dB was recorded for the composite foams, and this was 45% higher than the total SE value of solid nanocomposites (see Figure 5) [99]. The prime mechanism of shielding was also dominated by absorption of EM waves in the foamed nanocomposites. Nevertheless, via physical foaming, the density of the HDPE-GnP nanocomposites was also reduced by up to 26%, which opens up new avenues for designing lightweight EMI shielding materials at very low percolation thresholds.
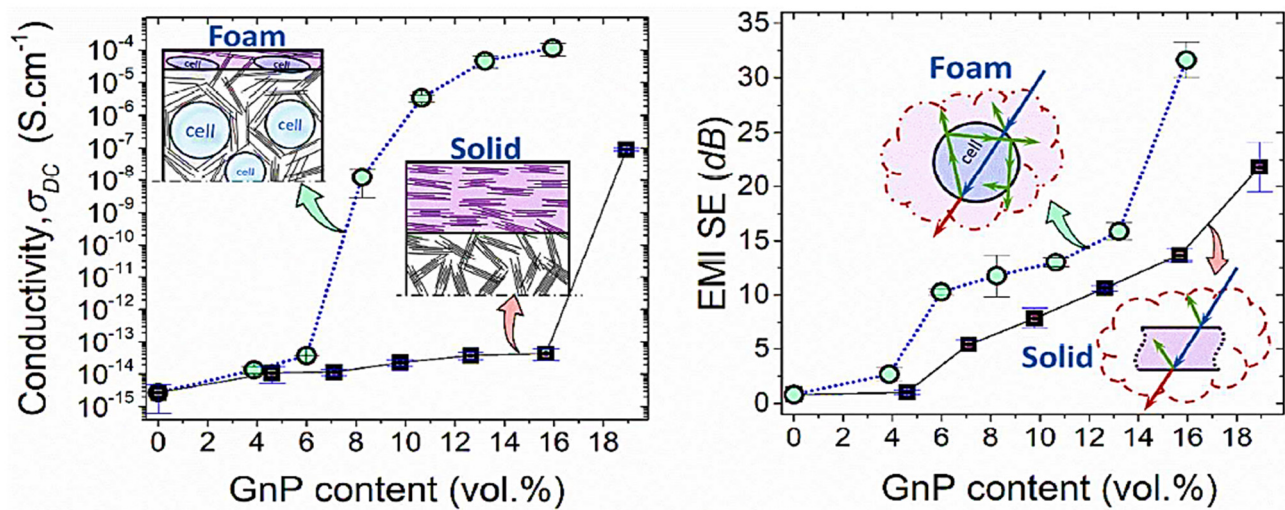
Figure 5. Variation of the electrical conductivity and the EMI SE value in solid and foamed HDPE-GnP composites. Reproduced with permission from [99]. Copyright 2018, American Chemical Society.

6. Measuring EMI Shielding Effectiveness (EMI SE) of Porous Polymer Nanocomposites

The most widely used instrument to measure the EMI SE of polymeric nanocomposite shields is placing the test samples inside the waveguide of a Vector Network Analyzer (VNA), where one can measure both the magnitude and phase of the EM signals. However, by using a Scalar Network Analyzer (SNA), one can only measure the magnitude of the signals and cannot measure the complex permittivity and permeability of test specimens. Hence, VNA is the most preferred instrument to elucidate the shielding performance. The incoming and transmitted EM waves from a two-port VNA can be expressed in terms of scattering parameters (viz. S_{11}, S_{21}, S_{22}, S_{21}), where S_{11} and S_{21} are forward reflection and transmission coefficients, and S_{22} and S_{21} are reverse reflection and transmission coefficients. As per the EMI shielding theory, the relation between power coefficients of reflectance (R), absorbance (A) and transmittance (T) is expressed as [100]:

$$A + R + T = 1 \tag{15}$$

where

$$T = |S_{12}|^2 = |S_{21}|^2 \tag{16}$$

$$R = |S_{11}|^2 = |S_{22}|^2 \tag{17}$$

The EMI SE can be calculated using the following equations [100]:

$$SE_R = -10 \log(1 - R) \tag{18}$$

$$SE_A = -10 \log\left(\frac{T}{(1 - R)}\right) \tag{19}$$

$$SE_{Total} = SE_A + SE_R + SE_{MR} = -10 \log T \tag{20}$$

Herein, SE_{MR} is the shielding due to multiple internal scatterings which can be neglected when $SE_A \geq 10$ dB [101].

7. Methods to Fabricate Polymer Foams and Aerogels

Polymer foams are mostly fabricated with the addition of chemical blowing agents, which release gases into the bulk polymer matrices due to a reaction that is mostly exothermic in nature. If the entrapped gas attains roughly spherical and separate pores, it results in the formation of a rigid closed-cell foam. Meanwhile, if the pores are well-interconnected, it gives rise to flexible open-cell foam. The open-cell foams are mostly used as upholstery

and acoustic insulation, whereas closed-cell foams are widely utilized for thermal insulation. There are several industrial techniques for the production of thermoplastic foams, viz. batch foaming, foam extrusion and foam injection molding [102]. The selection of a particular foaming process depends on the final product and end application of the foam. Moreover, the use of chemical blowing agents may lead to contamination as undesired residues can remain in the matrix even after the foaming process. Hence, physical blowing agents are more desirable for creating porous networks. Currently, the main focus is on the usage of supercritical CO_2 due to its non-flammability, chemical inertness, efficient process control, relative ease of handling and good interaction with polymers compared to other inert gases [103]. Moreover, it expediently replaces conventional volatile solvents, viz. chlorofluorocarbons (CFCs), butane or pentane, which are infamous for their contribution to the depletion of the ozone layer. Therefore, next-generation polymer-based EMI shielding foams are preferably manufactured by the CO_2-aided technique.

Aerogels are a class of porous solids which possess extremely low density, high surface area and tunable porosities (90–99%) that can be prepared from various polymeric precursors by sol–gel method and subsequent freeze/supercritical drying to remove the solvents from the wet gels and replace them with air [104]. However, aerogels possess even higher porosity and lower densities than polymeric foams and are hence suitable for high-end technological applications such as sensors, energy storage, biomedical scaffolds and many more [105]. The higher production cost associated with aerogel fabrication is the main drawback that restricts its commercial application. Depending on the morphology, aerogels can be further classified as isotropic and anisotropic aerogels. A rapid immersion of the polymer precursor into liquid N_2 will arrest the molecular motions within the solution, thereby preserving its original structure. This results in the formation of isotropic aerogels. However, when we adopt slower freezing of the precursor solution on copper plates using liquid N_2, it leads to the formation of anisotropic aerogels. This technique is also known as unidirectional ice templating (IT) [104]. In this process, the ice crystals slowly start to grow in one direction, which results in the formation of 2D pores/cells that are aligned parallel to the freezing direction, which eventually results in a honeycomb-like structure in the aerogels. In this review, we primarily focus on the fabrication of various conductive polymer nanocomposite aerogels and foams that can deliver high EMI shielding performance.

8. Elastomer Nanocomposite Foams for Electromagnetic Interference Shielding

Owing to their superior compressibility and flexibility, elastomer-based nanocomposite foams have been widely explored for their EMI shielding ability and microwave absorption performance. Amongst elastomers, silicon rubber, natural rubber and butadiene rubber have been converted into three-dimensional porous foams by using chemical/physical blowing agents or via the supercritical carbon dioxide (Sc-CO_2) foaming technique. Yang et al. [106] fabricated flexible and very lightweight methyl vinyl silicon rubber (VMQ)/multi-walled carbon nanotubes (MWCNTs)/ferriferous oxide (Fe_3O_4) nanocomposite foams using Sc-CO_2 foaming, as shown in Figure 6. The microwave-absorbing ability of these nanocomposite foams was found to be enhanced due to the formation of a porous structure, thereby considerably reducing the secondary EM pollution due to the reflection of microwaves. These flexible and compressible foams showcased low density (~0.48 $g.cm^{-3}$), with an average EMI SE of 27.5 dB and an average absorption efficiency of 64% in the X-band region (8.2–12.4 GHz) [106]. It was reported that, at 1.78 vol.% filler loading, a maximum electrical conductivity of ~14.6 S/m and specific EMI SE of ~72 $dB \cdot g^{-1} cm^3$ were achieved by using this process. It is also worth mentioning that the foams exhibited excellent EMI shielding stability, with a 96.2% retention of EMI SE even after 1000 bending cycles.
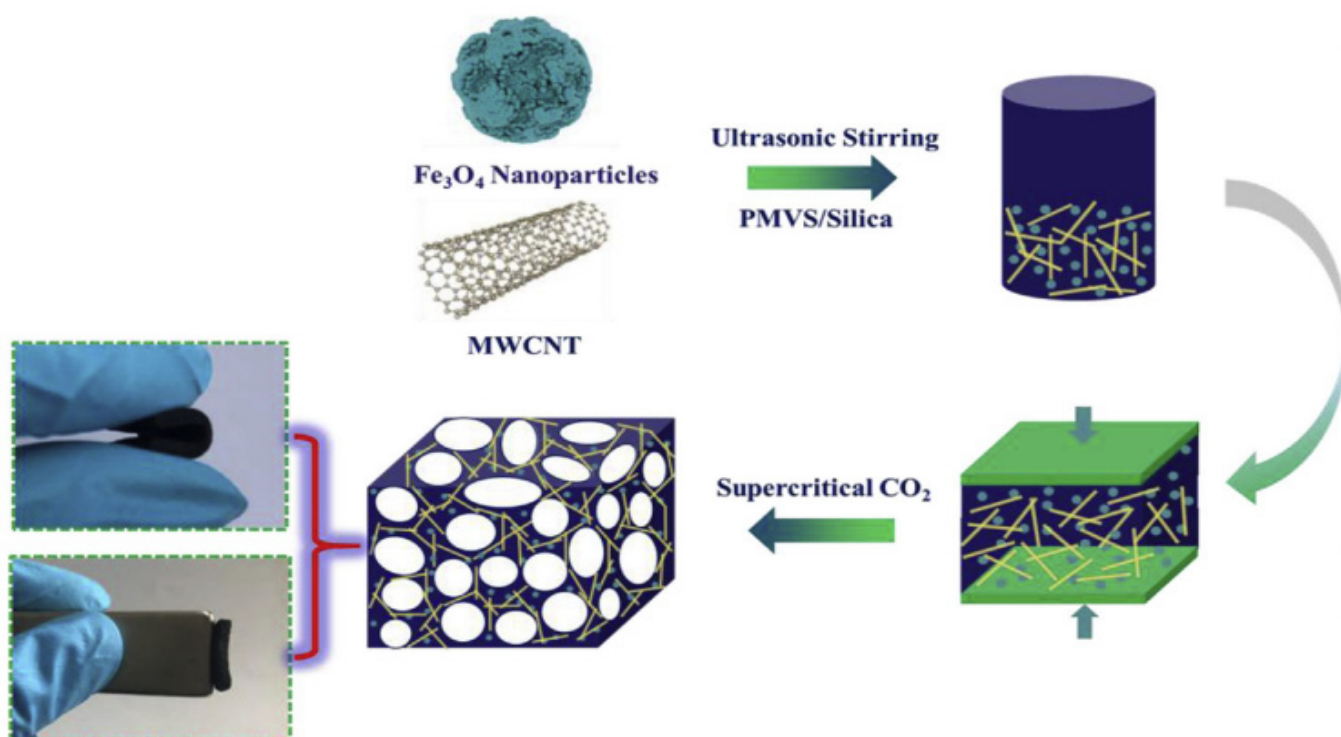
Figure 6. Schematic for the preparation of VMQ/MWCNTs/Fe3O4 nanocomposite foams. Reproduced with permission from [106]. Copyright 2019, Elsevier Ltd.

Backfilling an elastomer into a preformed three-dimensional (3D) conductive skeleton of nanofillers is yet another burgeoning approach for developing highly conductive elastomer nanocomposite foams. Li et al. [107] made use of this strategy to fabricate porous EMI shielding materials with enhanced microwave absorption properties. Herein, an elastomer matrix, i.e., polydimethylsiloxane (PDMS), was used to reinforce a highly conductive and robust three-dimensional bi-continuous skeleton of graphene/silver nanowires. Initially, GO suspension was added to AgNWs dispersion and homogenized to form stable hydrogels. This was followed by a thermal reduction of the hybrid hydrogel into rGO/AgNWs networks, which were eventually freeze-dried for 48 h to form 3D bi-continuous conductive structures. This porous network was then immersed in PDMS with a curing agent to form robust and compressible PDMS-reinforced GACs (PGACs), as shown in Figure 7A. The EMI shielding value of these hybrid foams reached 34.1 dB at 0.43 wt.% rGO and 0.33 wt.% AgNWs loading, and showcased superior conductivity of 10.6 S/cm and high specific EMI shielding effectiveness of 22.43 dB/unit filler wt.%/mm [107]. In addition, these monoliths demonstrated excellent compressibility, thermal stability and flame retardancy (see Figure 7B).

In another work, Zhao and co-workers developed flexible and high-performance EMI shielding foams from PDMS/rGO/SWCNTs nanocomposites using a similar backfilling approach by exploiting a preformed rGO/SWCNTs aerogel as a 3D conductive skeleton. These nanocomposite foams were fabricated based on a two-step process using GO and pristine SWCNTs, as shown in Figure 8. Initially, a sol–gel self-assembly of reduced GO and SWCNTs was performed, and they were subsequently freeze-dried to create a robust 3D rGO/SWCNTs aerogel skeleton. The next step was penetration of PDMS into the formed porous network, followed by the curing process. The 3D bi-continuous carbonaceous network in the foams created a highly efficient pathway for the electron transport and demonstrated high electrical conductivity of 1.2 S/cm, with a maximum EMI SE of 31 dB in the X-band region at very low loading of 0.28 wt.% rGO and SWCNTs [108].
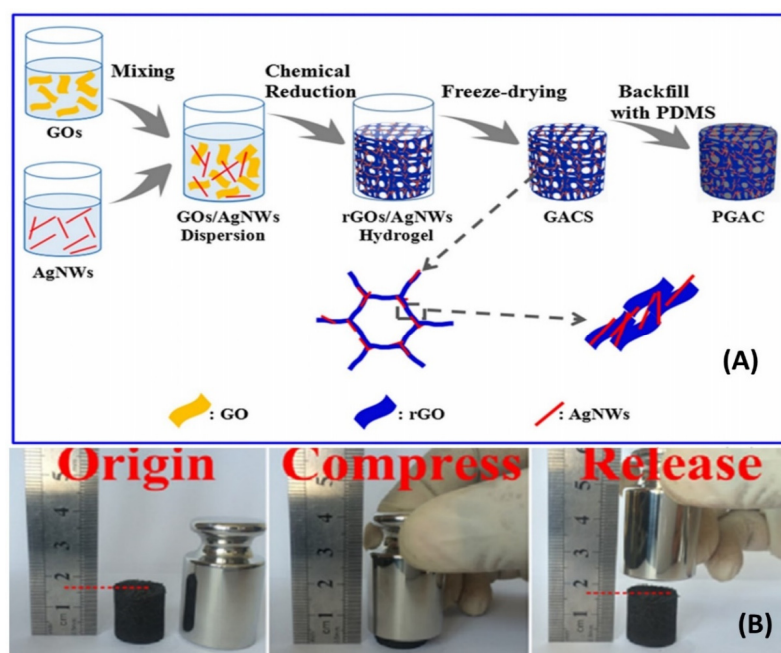
Figure 7. (**A**) Schematic demonstrating the fabrication process of hybrid RGO/AgNW/PDMS monoliths. (**B**) Compression test of hybrid monolith. Reproduced with permission from [107]. Copyright 2019, Elsevier Ltd.
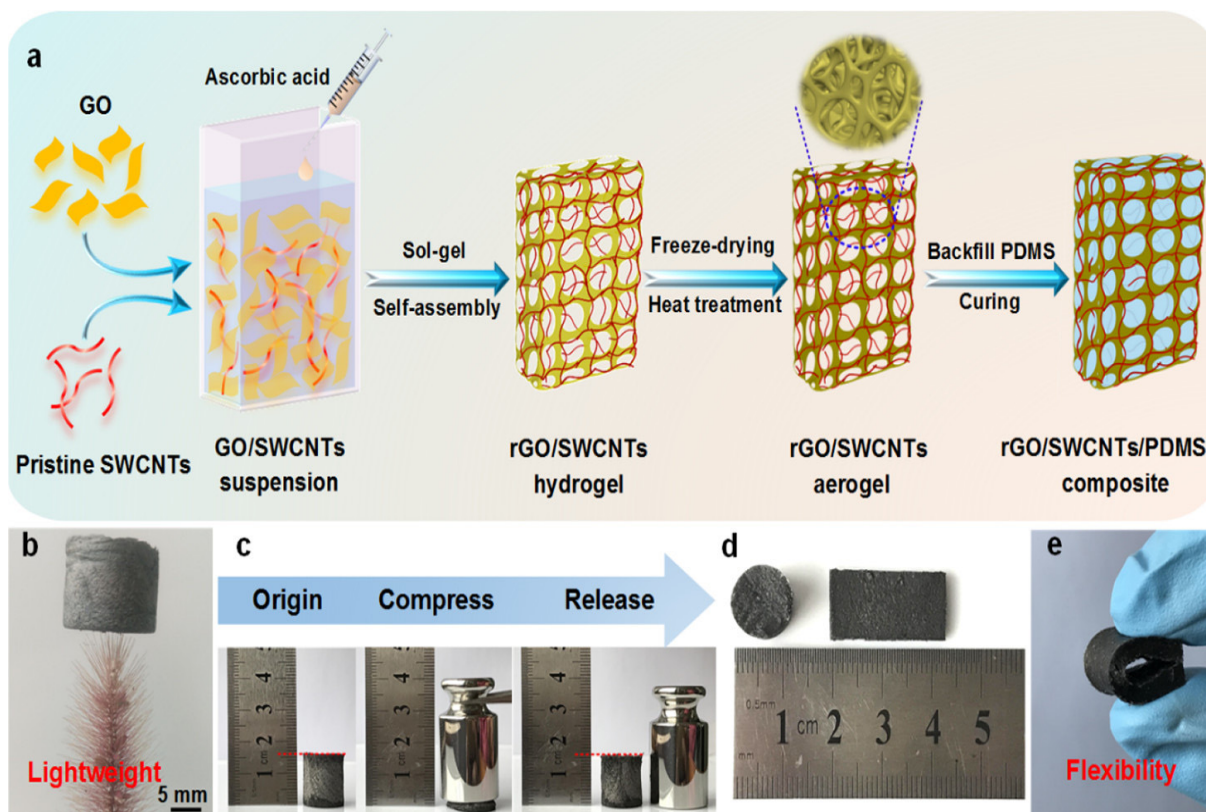
Figure 8. (**a**) Schematic depicting the fabrication of rGO/SWCNTs/PDMS aerogel. (**b**) Digital photograph of the ultralight aerogel. (**c**) A photograph of aerogels demonstrating excellent compressibility and super-elasticity. (**d,e**) Optical images of these aerogels in diverse shapes (**d**) and bending of aerogels demonstrating outstanding flexibility (**e**). Reproduced with permission from [108]. Copyright 2018, American Chemical Society.

9. Thermoplastic Foams for Electromagnetic Interference Shielding

Thermoplastic foams are widely used across diverse technological domains due to their lightweight nature, low thermal conductivity, high energy absorption and their superior strength/weight ratio. Owing to their excellent properties, thermoplastic foams have been utilized for building, construction, biomedical, automotive, sports, electronics and packaging applications. Fabrication of porous conductive thermoplastic nanocomposites with low density and high microwave absorption performance are very much favorable for practical device application. Chen et al. [109] fabricated porous and lightweight nanocomposites with segregated conductive networks of polystyrene (PS) and multi-walled carbon nanotube (MWCNT) by combining high-speed mechanical mixing and scCO$_2$ foaming. PS powder and MWCNT were subjected to high speeds of 28,000 rpm in a mixer, which generated static electricity to facilitate the coating of MWCNT on PS powders via electrostatic adsorption. The coated nanocomposite powder was then compression-molded at 160 °C, which resulted in the formation of a segregated conductive network, as shown in Figure 9a. The solid nanocomposite sheets were then subjected to foaming using scCO$_2$, which accords with the sustainable fabrication of PS/MWCNT foams. Interestingly, at 1.88 vol.% MWCNT loading and a very low thickness of 1.8 mm, these nanocomposite foams exhibited a very low density of 0.47 g/cm^3, electrical conductivity of 8.05 S/m and maximum EMI SE of 23.2 dB in the X-band region [109]. It is also worth mentioning that at the same MWCNT vol.% (i.e., 7%), the nanocomposite foam exhibited higher microwave absorption (95.9%) than the solid shields (90.5%). This enhancement and absorption-dominant shielding mechanism were ascribed to ohmic losses and polarization losses in PS/MWCNT foams. This is an environmentally friendly technique to fabricate high-performance microwave absorbers for next-generation electronic devices.
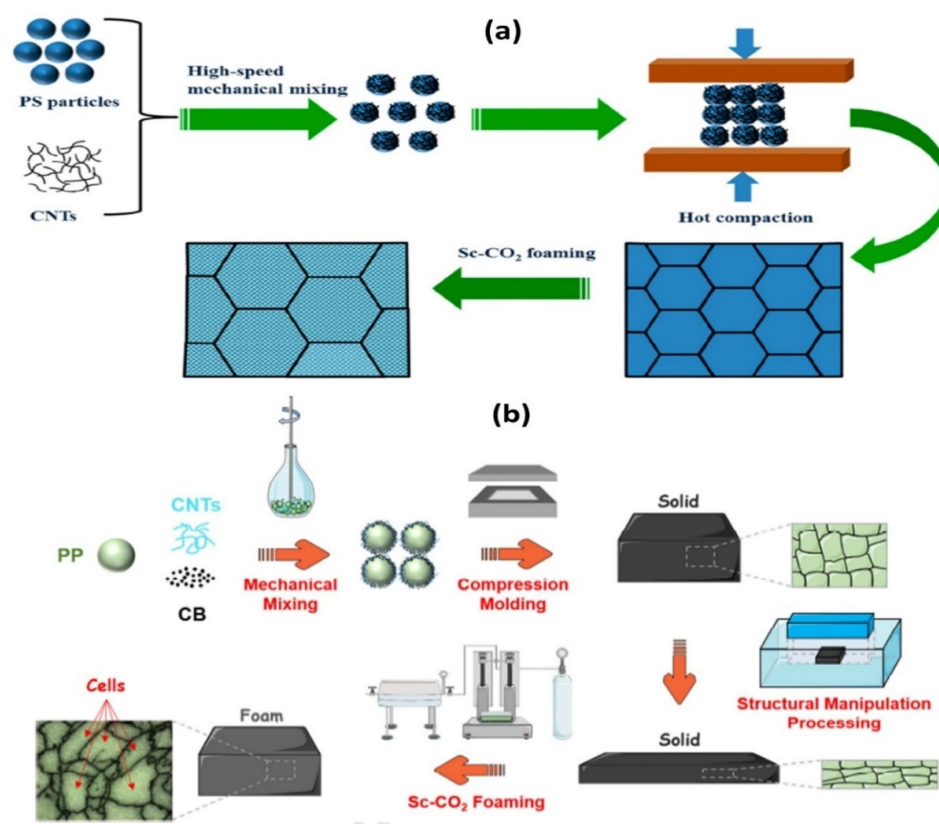
Figure 9. (**a**) Schematic depicting the fabrication of a segregated structure within porous PS/MWCNT composites. Reproduced with permission from [109]. Copyright 2019, American Chemical Society. (**b**) Schematic demonstrating the formation of a double-segregated structure within PP/CNTs/CB nanocomposite foams. Reproduced with permission from [110]. Copyright 2020, Elsevier Ltd.

Polypropylene is yet another thermoplastic polymer that is widely used to fabricate flexible and robust olefinic foams which have diverse applications in upholstery, roofing, construction, biomedical and automotive sectors. However, its application as an efficient high-performance microwave absorber is very limited and is yet to be discerned. Ju and co-workers made use of a similar strategy adopted by Chen et al., to fabricate lightweight polypropylene (PP)/carbon nanotubes (CNTs)/carbon black (CB) nanocomposite foams. Herein, PP powders were blended with CNT/CB powder at different weight ratios in a grinder at 20,000 rpm/min at 100 °C. In due course, the filler is adsorbed to PP due to electrostatic forces, coupled with the surface heating effect. The blended powder compositions were then compression-molded at 180 °C, which resulted in the formation of a highly conductive segregated network, which was eventually foamed into porous PP/CNT/CB nanocomposites, as shown in Figure 9b. These porous foams showcased a very low density in the range of 0.082–0.101 g/cm^3 and an extremely low percolation threshold of 0.016 vol.%, which was likely due to the hybrid combination of the fillers. A maximum of 20 dB EMI SE value was attained at a 2.5 mm thickness, with specific EMI SE as high as 72.23 dB·cm^3/g with an absorption-dominant shielding behavior [110].

10. Polyurethane Foams for Electromagnetic Interference Shielding

Polyurethane foams are synthetic porous materials with excellent physicochemical properties, high compressive strength, excellent chemical resistance and ease of processability, which makes them an ideal candidate for a wide range of applications in emerging sectors, such as high-frequency electronics, aerospace and automobile sectors. PU foams with tailor-made properties can be achieved by altering the ratio of hard and soft segments, polydispersity, molecular weight and also the degree of crosslinking. The presence of strong hydrogen bonding in polyurethane creates linkages between polymer chains, which in turn enhances the overall mechanical properties of PU foams. The increasing demand for high-performance and lightweight materials has motivated researchers to fabricate porous architectures by incorporating nanofillers such as carbon nanotube (CNT), carbon nanofibers and graphene. Mostly, these nanofillers are introduced into polyol, chain extender or prepolymer during PU synthesis, before adding the foaming agent. The resulting conducting polyurethane nanocomposite foams have been exploited for a plethora of applications, such as oil absorption, thermal insulation, sensors and EMI shielding. Li et al. [111] fabricated a series of multilayered thermoplastic polyurethane/graphene (PUG) composites by stacking single-layered PUG foams one above the other. By arranging PUG foams in different orders, they could realize a gradient in the concentration of graphene, which in turn enhanced the microwave absorption performance of PUG composites, without significant changes in their EMI SE values. Figure 10a shows the strategy adopted to fabricate large-scale manufacture of PU/graphene nanocomposite foams. Sandwiching PUG foams in a particular fashion was also another approach which was found to be more advantageous in improving the EMI SE values of these foams, and an optimized design also enabled the PUG foams to absorb more than the gradient foams. A maximum EMI SE of 24 dB was obtained at 18 GHz, with minimal reflection of EM waves [111].

Another approach adopted by Jiang et al. [112] was to fabricate porous thermoplastic PU/graphene oxide nanocomposite foams without the usage of any organic volatile solvents or a solution mixing process. Initially, TPU-coated RGO powders were prepared by mixing TPU particles in GO suspension with ascorbic acid and in situ reduction of GO to form TPU/RGO powders. These nanocomposite powders were then compression-molded into sheets by subjecting to 10 MPa at 120 °C for 10 min to generate a segregated network structure, as shown in Figure 10b. The solid nanocomposites sheets were then exposed to scCO$_2$ to fabricate porous TPU/RGO nanocomposites. At 3.71 vol.%, solid TPU/RGO nanocomposites showcased a higher EMI SE value of 24.7 dB, whereas porous nanocomposites recorded only 21.8 dB, with much higher absorption characteristics and minimal reflection [112]. It is also worth mentioning that there was only a slight decree of 5 dB in the

attenuation of TPU/RGO nanocomposites, even after 100 bending cycles, which portrays the efficiency of the segregated network structure in these nanocomposites.
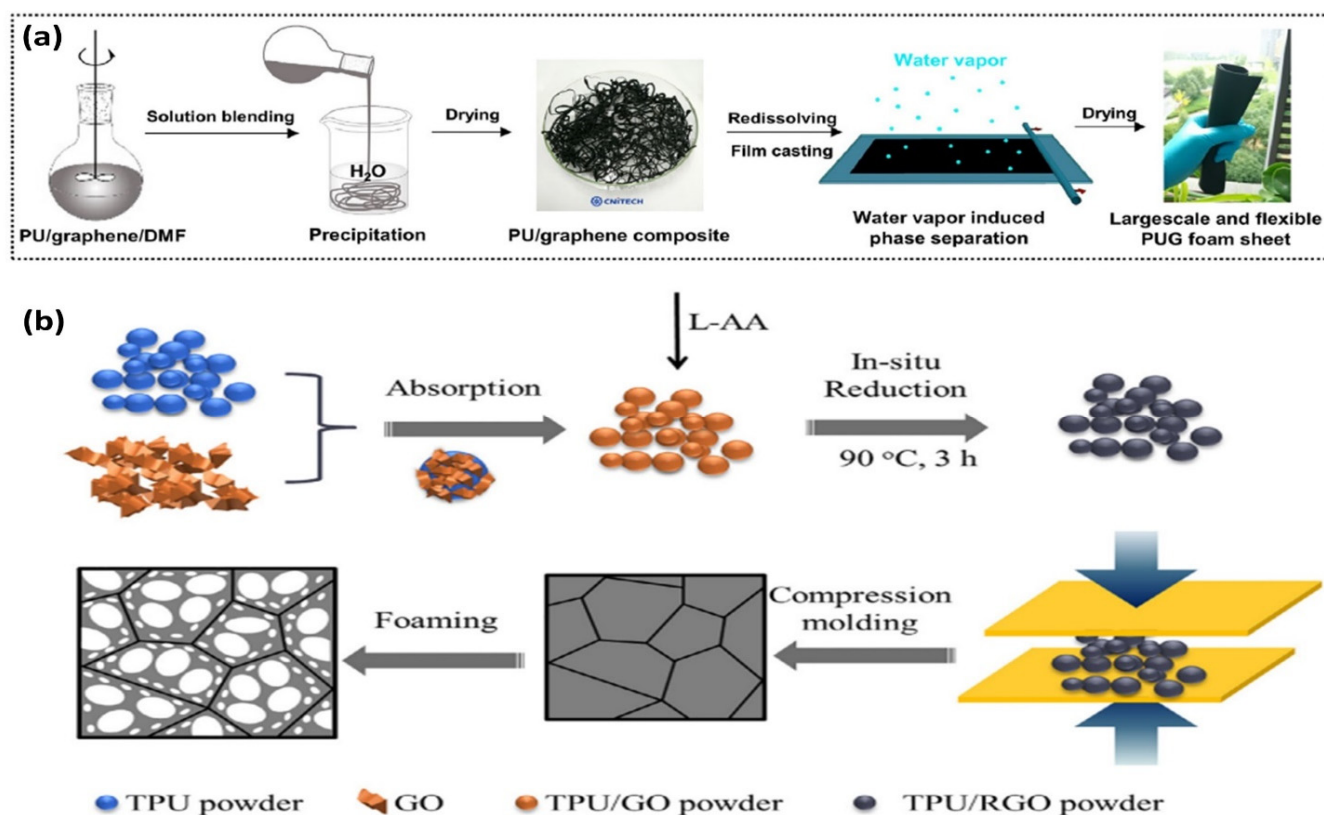
Figure 10. (**a**) Schematic depicting the fabrication process of PU-graphene foams. (**b**) Schematic showing the preparation technique of TPU/RGO composite foams. Reproduced with permission from [111,112]. Copyright 2019, 2017 Elsevier Ltd.

All the aforementioned protocols require multiple steps to fabricate and design porous polymer nanocomposites. Hence, it is quite necessary to formulate a process which is facile and scalable at the same time. In this view, Shen et al. [113] developed conductive, ultralight and compressible PU foams by facile solution dip-coating of graphene onto commercially available PU foams. The resultant PU/graphene foams exhibited very low density of ~0.027–0.030 g/cm^3 and demonstrated superior broadband EM attenuation performance with an absorption-dominant shielding mechanism. Figure 11 depicts the dipping process, coating uniformity, morphology and compressive nature of the PU/graphene nanocomposite foams. A maximum EMI SE value of 39.4 dB was recorded at 12 GHz and 6 mm thickness [113]. Moreover, owing to their outstanding compressibility, the shielding performance of the PU/graphene foams could be fine-tuned by mechanical compression, which endows its adjustable EMI shielding characteristics. In addition, these foams also exhibited good cycling stability with stable EMI values even after 50 compression cycles, and demonstrated huge prospects for large-scale production of PU-based microwave absorber foams.
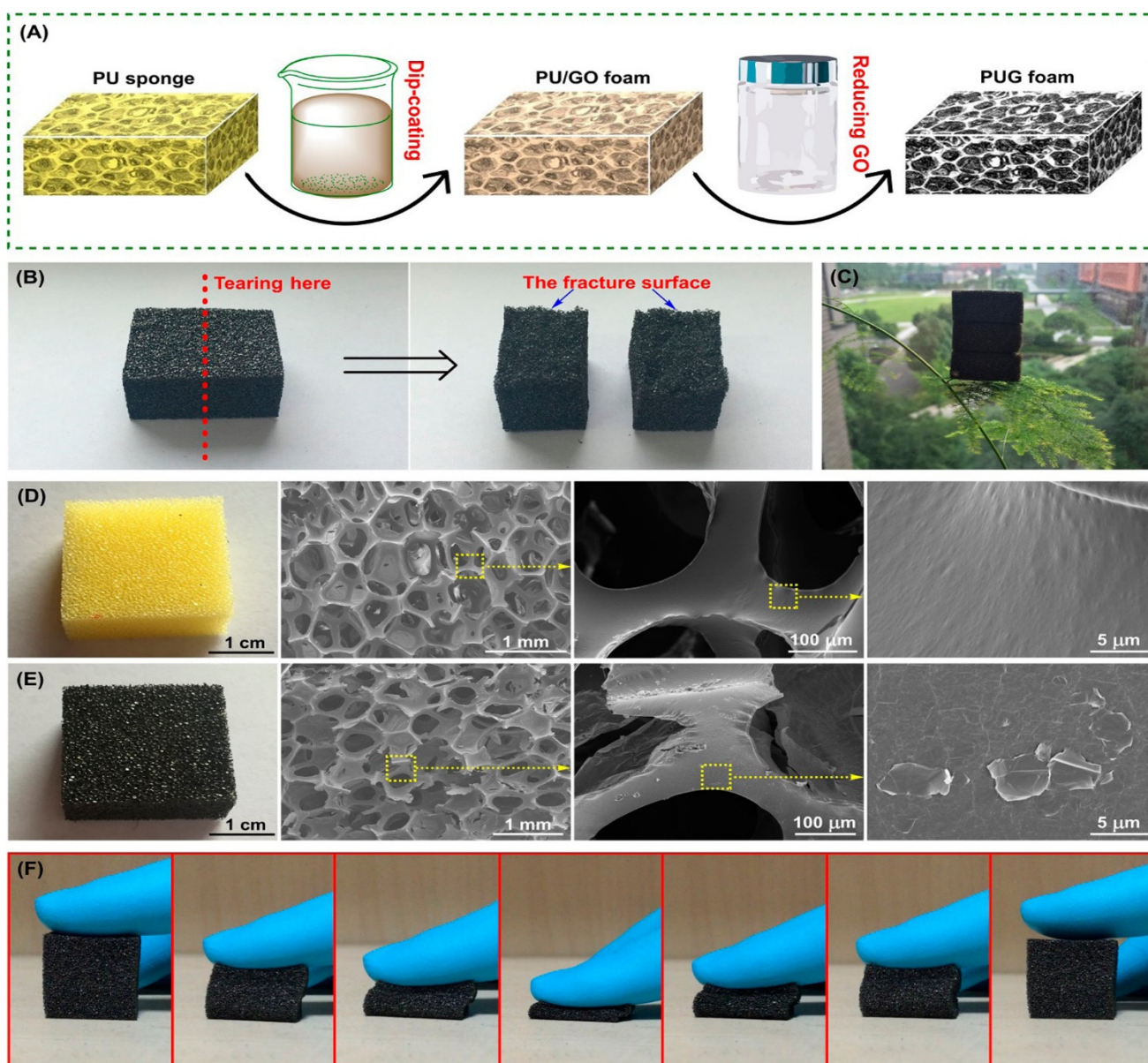
Figure 11. (**A**) Stepwise fabrication process of PU/graphene foams, including dip-coating GO sheets onto PU foams followed by hydrothermal reduction using hydrazine vapor. (**B**) A piece of foam showing uniform coating after being torn from the middle portion. (**C**) A block of foam on the leaf of an asparagus fern. (**D**,**E**) Optical and SEM images of pristine PU sponge and PU/graphene foam. (**F**) Compressing and releasing these foams depicting excellent compressibility and recovery. Reproduced with permission from [113]. Copyright 2016, American Chemical Society.

11. Bioplastic Foams for Electromagnetic Interference Shielding

The replacement of conventional fossil fuel-derived synthetic polymeric foams with bio-sourced, biodegradable and sustainable alternatives will be crucial for promoting a circular economy. Synthetic foams such as polystyrene (PS) and polyolefin foams end up as landfill after their lifecycle and are estimated to remain in soil for generations and wreak havoc on the environment. Recently, much attention has been focused on PLA, which is a linear aliphatic polyester sourced from renewable feedstocks such as corn, potato, sugar and other agricultural sources.

In general, there are three types of PLA, viz. poly(D-lactic acid) (PDLA), poly(L-lactic acid) (PLLA) and a racemic blend of D,L-PLA (PDLLA). Nowadays, a majority of sustainable research is inclined towards poly(lactic acid) (PLA) foams and they are

being widely explored as promising biodegradable substitutes for synthetic foams, which currently own a major stake in the industry. This is primarily due to the ease of processing, good barrier and mechanical properties of PLA, accompanied by their environmentally friendly nature. Besides the packaging industry, there are huge prospects for PLA foams for use in biomedical, energy, sensors and EMI shielding applications. In this context, Wang et al. [114] fabricated a facile and eco-friendly route for the large-scale production of biodegradable and ultra-low-threshold PLA/MWCNT porous nanocomposites for superior thermal insulation and EMI shielding. Herein, PLA beads were foamed using a bead-foaming process to obtain expanded PLA (EPLA) beads, followed by mechanical mixing with (0.25–2.5 wt.%) MWCNT dispersion. This resulted in a uniform coating of MWCNT onto EPLA beads, which were then sintered together by the steam-chest molding process to fabricate bulk PLA/MWCNT porous nanocomposites with 3D segregated MWCNT networks distributed between the EPLA pellets, as shown in Figure 12A. It also worth mentioning that porous nanocomposites fabricated in this fashion exhibited an ultra-low percolation threshold of 0.00094 vol.% and a density of 0.045 g/cm^3, as seen in Figure 12B. A maximum EMI SE value of ~50 dB was recorded at 8 GHz, and a specific EMI SE value of 1010 dB·cm^3·g^{-1} [114]. Moreover, the shielding mechanism in these porous structures was primarily governed by absorption of incident EM waves.
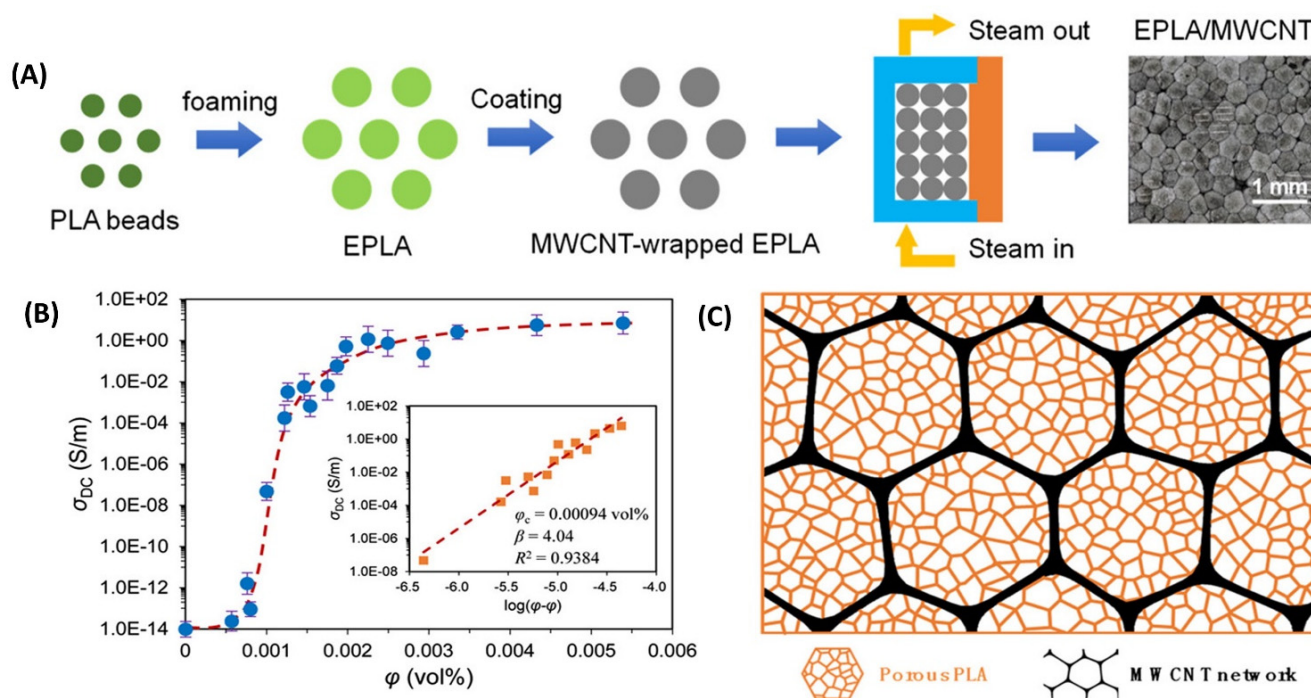
Figure 12. (**A**) Schematic representation of the fabrication technique used to design segregated MWCNT networks in porous PLA/MWCNT foams. (**B**) Variation of the electrical conductivity of these foams with respect to MWCNT content. The inset plot shows σ vs. (φ − φ$_c$). (**C**) Schematic illustration of the segregated 3D conductive networks of MWCNTs at the periphery of EPLA beads. Reproduced with permission from [114]. Copyright 2017, American Chemical Society.

However, PLA exhibits relatively less heat resistance and can hardly be used in extremely hot conditions above 100 °C. Therefore, to enhance the thermal stability of PLA foams, another strategy that was adopted by Cui and coworkers is creating stereo complex crystallites (sc) between enantiomeric poly(L-lactide) (PLLA) and poly(D-lactide) (PDLA) via stereo complexation crystallization. Initially, CNT was homogeneously dispersed in the PLLA/PDLA/dichloromethane (DCM) solution by ultrasonic dispersion and mechanical mixing. Hexane was then added dropwise to promote the formation of stereo complex crystallites, which will then form a 3D network-like structure due to gelation. The porous

PLLA/PDLA/CNT foams were then prepared via a non-solvent-induced phase separation and freeze-drying, as shown in Figure 13. The CNT/scPLA foam with 1.48 vol.% CNT demonstrated a lower foam density of 0.10 g/cm^3 and a maximum EMI SE value of 21.6 dB, as well as a specific EMI SE value as high as 216 dB·cm^3·g^{-1} [115]. It was also observed that the formation of stereo complex crystallites with a high crystallinity of ~45% and well-interconnected CNT networks portrayed good dimensional stability of PLA foams, with only minimal shrinkage of 4.3% at 220 °C.
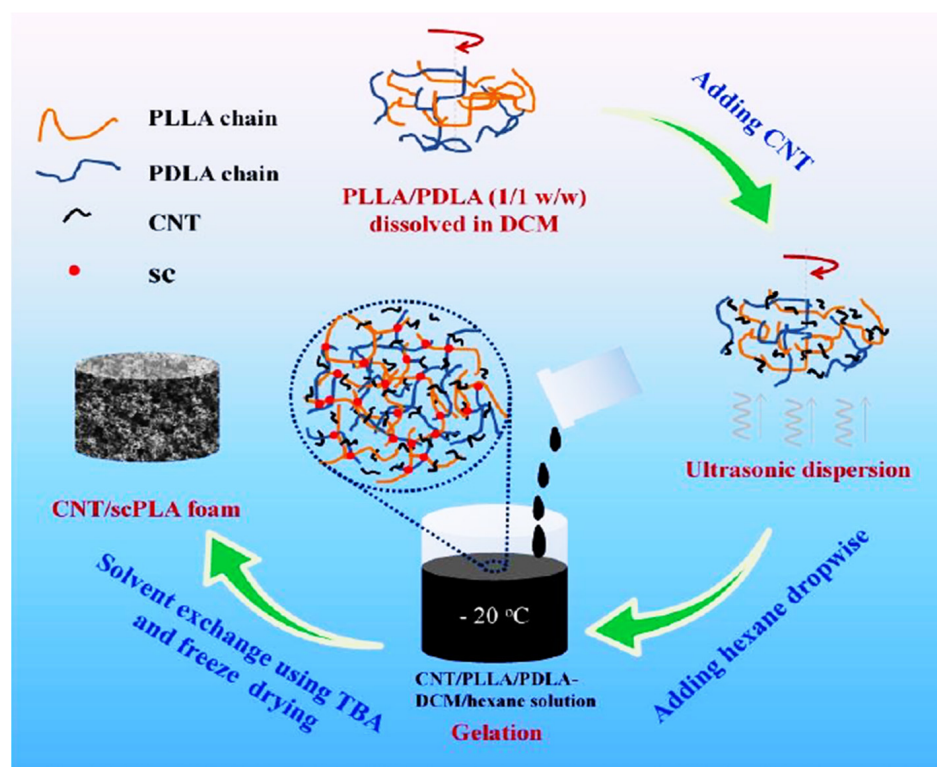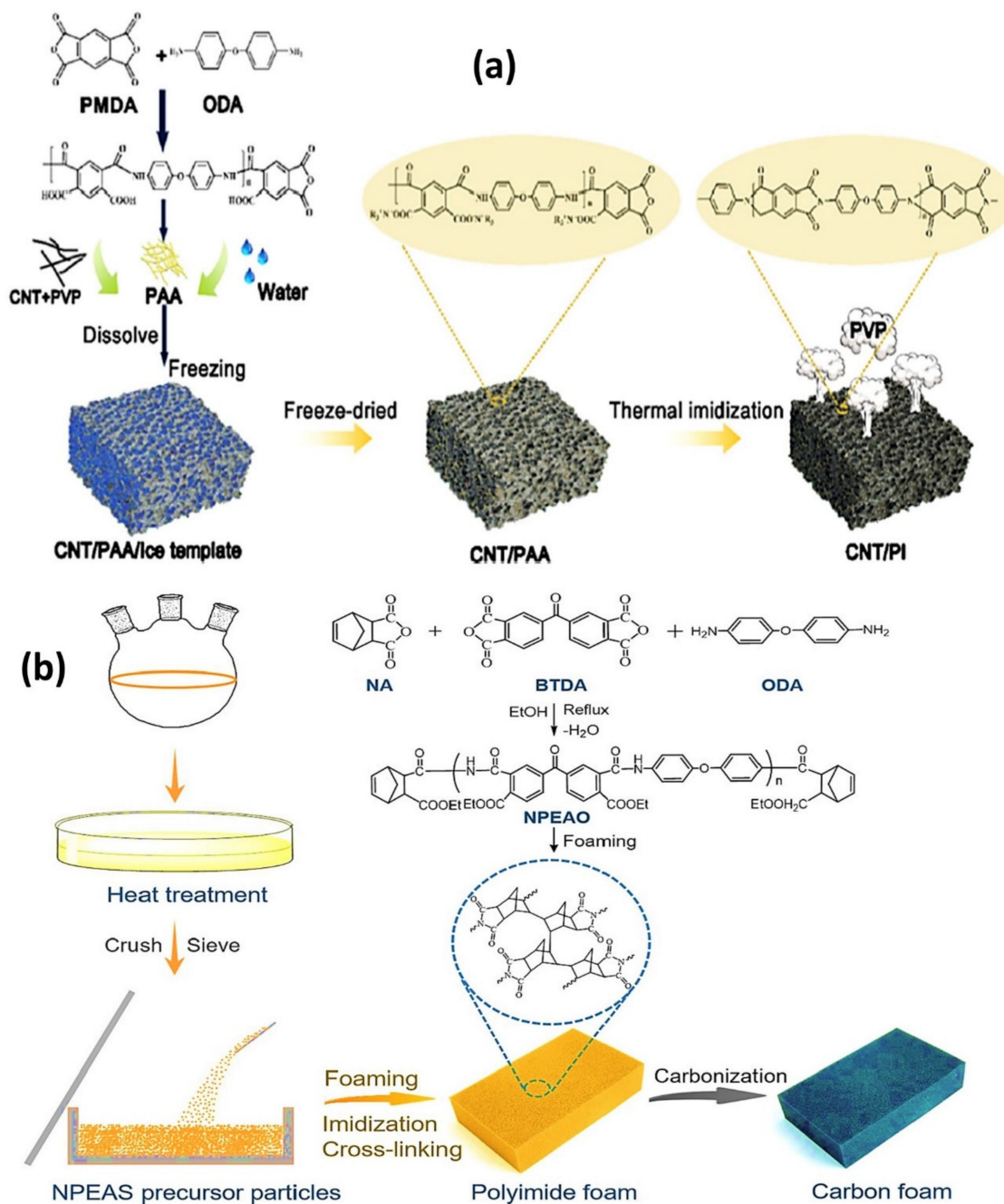

Figure 13. Schematic demonstrating the fabrication process of PLA/CNT foams. Reproduced with permission from [115]. Copyright 2017, Elsevier Ltd.

12. Porous Polyimide Nanocomposites for Electromagnetic Interference Shielding

Polyimides (PI) are a class of high-performance polymer materials which contain the imide group (-CO NHCO-) in the chain backbone. They are well-known for their excellent mechanical strength, creep resistance, thermo-oxidative stability, chemical resistance, superior electrical insulation and remarkable dielectric properties. Owing to these exceptional properties, polyimides find application in microelectronic devices, flexible electronics, aircraft composite structures, cryogenic insulation and radiation shielding films. The synthesis of polyimides generally proceeds via a two-step condensation reaction mechanism, preferably in melt or solution polymerization using aromatic diamines and aromatic tetracarboxylic dianhydrides. In the first step, a soluble polymer precursor, poly(amic acid) (PAA), is formed from the ring-opening reaction of the dianhydride with diamine, followed by ring closure (imidization) of PAA to form aromatic polyimides. Recently, there is a growing need for high-performance polymer foams, especially in the aerospace industry for applications such as fireproof panels, cryogenic tank insulation and energy absorbers, which has led to the use of polyimide foams to meet these requirements. Henceforth, researchers are also making efforts to develop robust PI nanocomposite foams for potential use as high-performance microwave absorbers in aerospace, satellite communication and military sectors. In this context, Wang et al. [116] fabricated an array of robust and lightweight polyimide (PI)/carbon nanotube (CNT) foams with superior microwave absorption and thermal resistance. Initially, aqueous CNT suspension was

stabilized with poly(vinyl pyrrolidone), and later ultrasonicated in different wt.% with PAA to form a homogeneous CNT/PAA solution, which was then freeze-dried to form CNT/PAA foam. These foams were heated at gradient temperatures of 150–300 °C to induce thermal imidization to form PI/CNT foam, as shown in Figure 14a. The foam exhibited an average EMI SE of 41.1 dB, an 82.3% absorption coefficient (A) and a foam density as low as 32.1 mg·cm^{-3} [116]. It is noteworthy that, even after subjecting these foams at 300 °C for 48 h, PI/CNT foams showed a 35 dB EMI SE value. The performance of PI nanocomposite foams portrays their tremendous application potential for use in the harsh condition requirements of aerospace, defense and military sectors.

Figure 14. (**a**) Schematic illustrating the preparation of PI/CNT foam. Reproduced with permission from [116]. Copyright 2020, American Chemical Society. (**b**) Schematic demonstration of the fabrication process of carbon foams from PI foam. Reproduced with permission from [117]. Copyright 2020, Elsevier Ltd.

Carbonization of polymeric foam/aerogel often results in superior electrical conductivity and an enhancement in the specific surface area, which has a tremendous impact on the overall microwave absorption performance. In order to elucidate the effect of carbonization, PI foams were converted to carbon foams by subjecting them to extremely high temperatures in the range of 1000–1200 °C. This strategy was employed by Li and coworkers, wherein they fabricated rigid PI foams from the starting monomers, as show in Figure 14b. The PI foams were then carbonized at different temperatures (600 to 1500 °C) for 1 h under an N_2 environment to yield carbon foams with a maximum electrical conductivity of 0.215 S.cm^{-1}. Interestingly, foams carbonized at 1500 °C demonstrated high volume shrinkage of 46%, which can be ascribed to the highly crosslinked structure of the precursor PI foams. These carbon foams had a density of 0.091 g·cm^{-3} and showed a superior EMI SE value of ~54 dB and specific EMI SE of 593.4 dB·cm^3/g, respectively, at 10 GHz and at a thickness of 2.0 mm [117]. It is also worth mentioning that no conductive nanofillers were used during the fabrication of carbon foams.

Numerous porous nanocomposite foams and aerogels have been comprehensively studied for their microwave absorption performance and EMI shielding ability. Table 2 summarizes the EMI shielding properties (SE$_{Total}$, SSE), electrical conductivity, thickness, density and test frequency range of some porous nanocomposites studied in the literature.

Table 2. Measurement technique, shield thickness (mm), frequency (GHz), electrical conductivity (S/m), SE$_{Total}$ (dB) and specific EMI SE (dB.g^{-1}.cm^3) of some porous nanocomposites reported in the literature.

Sr No.	Aerogel/Foam Composition	Measurement Technique	Thickness (mm)	Density (g/cm^3)	Frequency (GHz)	Electrical Conductivity (S/m)	SE$_{Total}$ (dB)	Specific EMI SE (dB.g^{-1}.cm^3)	Ref
1	CNT sponge	waveguide	1.8	10.0	8–12	150–300	54.8	5480	[118]
2	CNT/PDMS	waveguide	2.0		8–12	150–300	46.3	-	[118]
3	rGO/epoxy composite	-	>0.1			~0.01	38	35.3	[119]
4	PEI/G@Fe3O4 foam	-		0.28−0.4	8−12		~41.5	-	[120]
5	GAF	coaxial	1.4	0.06	0.1–3	2.5 × 105	~135	-	[121]
6	GAF	coaxial	0.12	0.41	2–18	6600	70–105	-	[121]
7	GAs	waveguide	4	0.43	8–12	4.32	30	-	[122]
8	Ni-NiO/NCA	-	1.5	0.42	15.2		−41.9	-	[123]
9	carbon/Fe3O4@Fe	-	2		13–18		−49.6	-	[124]
10	CNT sponge	coaxial	2–3.5	0.02	1–18	278	20	1100	[125]
11	CNT/Epoxy composite	-	5–10	5	8–12	516	33	-	[126]
12	RGO/LDC Aerogel	waveguide	2	8.0	8.2–12.4	-	49.2	53,250	[127]
13	RGO/LDC Aerogel	waveguide	2	2.0	8.2–12.4	-	21.3	10,650	[127]
14	Graphene Aerogel	-	3	7.6	14.6	-	30.53	-	[128]
15	CF@G@PPy aerogels	-	3	8.8	9–12.6	-	40.59	-	[128]
16	GA-CT	-	2	0.07	-	-	27	371–385	[129]
17	GA-CT	-	3	0.07	-	-	37	514–528	[129]
18	CNTs/GNS@CoFe2O4	waveguide	3.0	0.095	8.2–12.4	-	29.1	-	[130]
19	epoxy/TGA	-	4		8–12	-	27	-	[7]
20	epoxy/TAGA (axial)	-	4		8–12	980	25	-	[7]
21	epoxy/TAGA (radial	-	4		8–12	96	32	-	[7]
22	Epoxy/pGAs	Coaxial	4	4.0	8–12	73	35	-	[131]
23	RGO/Ti3C2TX foam	waveguide	3.22	0.0033	8.2–12.4	-		14, 299.2	[132]
24	MXene aerogels	Waveguide	4	0.004	8.2–12.4	22	75	990	[133]
25	Ti3C2Tx MXene/ cellulose aerogel	Coaxial	2	0.31	11.2	-	−43.4	-	[121]
26	MXene Foams	-	3.2			58 00	≈70	-	[134]

Table 2. *Cont.*

| Sr No.	Aerogel/Foam Composition	Measurement Technique	Thickness (mm)	Density (g/cm^3)	Frequency (GHz)	Electrical Conductivity (S/m)	SE$_{Total}$ (dB)	Specific EMI SE (dB.g^{-1}.cm^3)	Ref
27	Graphene/PDMS foam	coaxial	~1	0.06	1.5–30	200	~30	500	[135]
28	GN/CNA	coaxial	2	52.1	8.2–12.4	19.1	58.4		[136]
29	Polypropylene/carbon fiber composite foams	Coaxial	-	-	8.0–12.4	-	24.9	-	[137]
30	Porous graphene/polystyrene foam composite	-	2.5	0.45	8.2–12.4	1.25	29	64.4	[138]
31	Polypropylene/ stainless-steel fiber composite foams	Coaxial	-	-	8.2–12.4	-	47.6	75	[139]
32	Silver Nanowire Hybrid Polyimide Composite Foams	Waveguide	5.0	0.014–0.022	30 MHz–1.5 GHz	-	17	772	[140]
33	Polyimide/reduced graphene oxide	Waveguide	0.8	0.28	8.2–12.4	0.8	17-21	75	[141]
34	Graphene foam/ poly (3,4-ethylenedioxythiophene): poly(styrenesulfonate) Composite	Waveguide	-	0.0182	8.2–12.4	43.2	91.9	3124	[142]
35	Polyetherimide/ graphene@Fe3O4 composite foams	Waveguide	2.5	0.28–0.4	8.2–12.4	-	14.3–18.2	41.5	[120]
36	Reduced graphene oxide/waterborne polyurethane composites	coaxial	1	-	8.2–12.4	16.8	34	-	[143]
37	PU/(rUL-GO) foam	Waveguide	-	0.053–0.092	8.2–12.4	4.04	20	253	[144]
38	Fluorocarbon/ MWCNT foam	Waveguide	3.8	1.2	8.2–12.4	-	50	-	[145]
39	Polypyrrole and reduced graphene oxide	Coaxial	1.5–5	-	2–18	-	−54.4	-	[146]
40	Natural rubber/ magnetic iron oxide (Fe3O4) and reduced graphene oxide	-	1.6	-	8.2–12.4	6.1	42.4	26.4	[147]
41	Multilayered thermoplastic polyurethane/graphene composite foams	Waveguide	6.5	0.42	12–18	3	24	-	[111]
42	Polymer-derived ceramic aerogels (PDCA)	Coaxial	2-4.5	0.19	2–18	-	−43.37	-	[148]
43	Polystyrene/ functionalized graphene nanocomposite foams	-	-	-	8.2–12.4	0.1	18	-	[149]
44	polycarbonate/ graphene nanocomposite foams	Waveguide	-	-	8.2–12.4	-	-	39	[150]
45	Epoxy/functionalized multi-walled carbon nanotube microcellular foam	Waveguide	2.5	-	12–18	1.04×10^{-5}	20.5	-	[151]
46	PP/CNT Foam	Waveguide	8	0.87	25–40	3.93	30–35	-	[152]
47	PVDF/graphene nanoplatelet composites	Waveguide	2.5	-	26.5–40	0.52	27	-	[15]
48	Graphene nanoplatelets/ carbon nanotubes/ polyurethane composites	Waveguide	3	-	12.4–18	$\sim 10^{-2}$	−47	-	[153]

13. Nanocellulose Aerogels for Electromagnetic Interference Shielding

Cellulose is one of the most abundant polysaccharides on the planet and is a key component present in the cell wall of plants. Basically, it is a linear biopolymer composed of 1,4-anhydro-D-glucopyranose units and is considered as a replenishable feedstock which has the potential for meeting the increasing demand for green and sustainable products. By virtue, cellulose has a fibrillar structure and coexists with hemicellulose and lignin in the plant cell walls. Inside individual cellulose fibrils, there exists regions that are highly ordered (crystalline) and disordered (amorphous), with strong inter/intra-molecular hydrogen bonding between the hydroxyl groups present in the cellulose backbone. At the nanoscale level, each macro-cellulose bundle is composed of several elementary cellulose nanofibers (5–20 nm diameter) that can be extracted and utilized for many technological applications, such as water purification membranes, substrates for flexible electronics, electrode materials for batteries and biomedical scaffolds [154]. These applications are made possible because of the excellent physicochemical properties of nanocellulose, such as high stiffness, high crystallinity, tunable surface chemistry and impeccable film-forming ability. However, for designing lightweight and robust solutions to the current challenges that the industries are facing, cellulose nanofiber (CNF)-based aerogels have gained much attention. CNF aerogels are highly porous solids with high porosity, ultra-low density and high specific surface area, and are foreseen as a feasible solution for advanced applications ranging from oil absorbents to biomedical scaffolds. In this view, Zeng et al. [155] developed a series of CNF aerogels decorated with silver nanowires (AgNWs) with minimal density and flexibility for high-performance EMI shielding. Herein, three different aerogel morphologies were fabricated using bidirectional, unidirectional and randomly directional freeze-casting methods using facile ice-templated freezing. Figure 15 depicts some of the key findings, such as the hierarchical structure of CNF, the Tyndall effect confirming the dispersion stability of CNF in water, different freezing approaches employed for making anisotropic and honeycomb-like aerogels, interactions of CNF and AgNWs, different aerogel morphologies and the bendability/twistability of CNF/AgNW aerogels. These aerogels demonstrated a maximum EMI SE value of 70 dB, with the highest specific EMI SE value of 178,235 dB·cm^2.g^{-1}, which far exceeds the values reported for biobased aerogels [155].

Upon addition of magnetic nanoparticles, one can enhance the overall permeability values of the nanocomposites, which can lead to enhanced microwave absorption. This approach was used by Chen and coworkers for fabricating cellulose/rGO/Fe$_3$O$_4$ aerogels by decorating Fe$_3$O$_4$ nanoparticles within the porous network of these aerogels. The steps involved in the fabrication of these aerogels are shown in Figure 16. Cellulose was dissolved in a sodium hydroxide/urea/H$_2$O mixture along with calculated amounts of graphene oxide (GO). Vitamin C solution (30 g/L) was used to reduce GO to form cellulose/rGO hydrogel, which was later freeze-dried for 48 h to form cellulose/GO aerogels. These hydrogels were also simultaneously immersed in an aqueous FeCl$_3$ and FeCl$_2$ solution to form Fe$_3$O$_4$-decorated hydrogel and lyophilized in a freeze drier to form cellulose/rGO/Fe$_3$O$_4$ aerogels. In order to elucidate the effect of porosity, film samples of these compositions were also fabricated. A maximum EMI SE value of 52.4 dB was achieved at a 2.0 mm aerogel thickness at 10 GHz [156]. With the increasing magnetic content and thickness of these aerogels and films, shielding by absorption was also found to increase. It is worth mentioning that aerogels showcased more shielding performance than films for same compositions, which can be ascribed to the porosity and the multiple filler polymer interfaces within the porous structure that facilitate more internal scattering of microwaves.

In situ coating of the CNF surface with intrinsically conducting polymers is yet another approach that can be utilized to fabricate high-performance microwave absorbers. This approach was utilized by Pai et al. [157] for fabricating ultralight and ultra-fast heat-dissipating PANI/CNF aerogels with 95% microwave absorption ability in X-band frequencies. Initially, in situ electro-oxidative polymerization of the aniline monomer was carried out in CNF suspension to stabilize hydrogels, which were later freeze-dried at

−80 °C for 48 h to obtain PANI/CNF aerogels, as shown in Figure 17. These aerogels demonstrated a maximum EMI SE value of −32 dB at 8.2 GHz and 5.0 mm thickness. It is noteworthy that owing to the very low density of 0.01925 g/cc, PANI/CNF showcased a high specific EMI SE value of ~1667 dB.g^{-1}.cm^3 and has huge application potential in telecommunication, military and defense sectors [157]. These aerogels also depicted ultra-fast heat dissipation behavior when exposed to high-power EM radiation inside a microwave oven, and could readily absorb excess EM energy emanating from electronic devices such as a mobile phone.
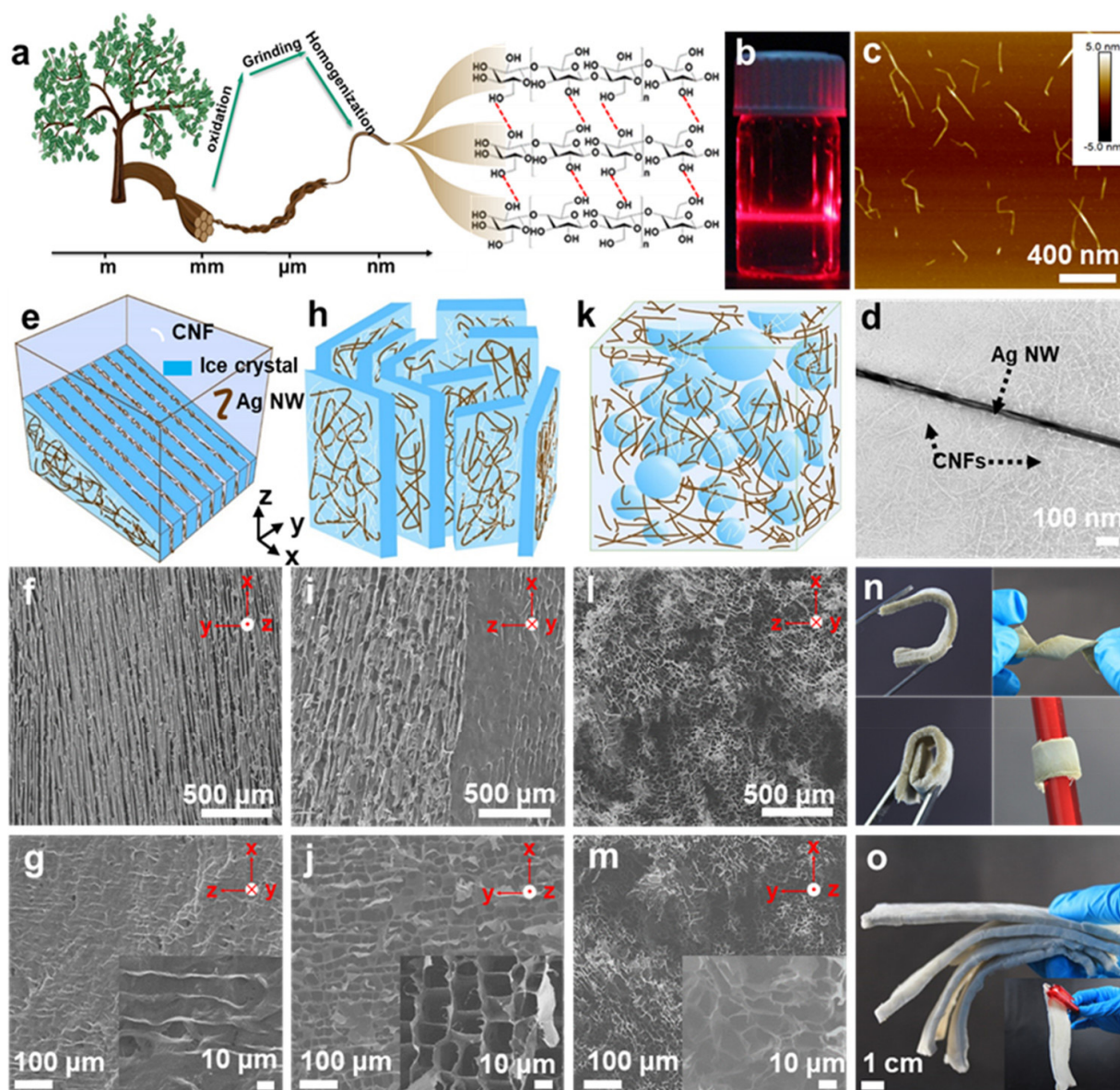

Figure 15. (**a**) Hierarchical structure of CNF and its preparation process. (**b**) Image of the CNF dispersion displaying the Tyndall effect. (**c**) AFM image of pristine CNFs. (**d**) TEM demonstrating good attraction and adhesion between the CNFs and AgNWs. Schematic representation of ice crystals' growth during various freezing approaches of the CNF/AgNW dispersion and SEM images of the resultant aerogels: (**e**–**g**) bidirectional, (**h**–**j**) unidirectional and (**k**–**m**) uniform/random freezing. (**n**) Bendability, twistability and rollability of these ultralight aerogels. (**o**) Demonstration of large-area lamellar porous CNF/AgNW aerogels with varying densities (inset, a large-area aerogel held up by electrostatic force). Reproduced with permission from [155]. Copyright 2020, American Chemical Society.
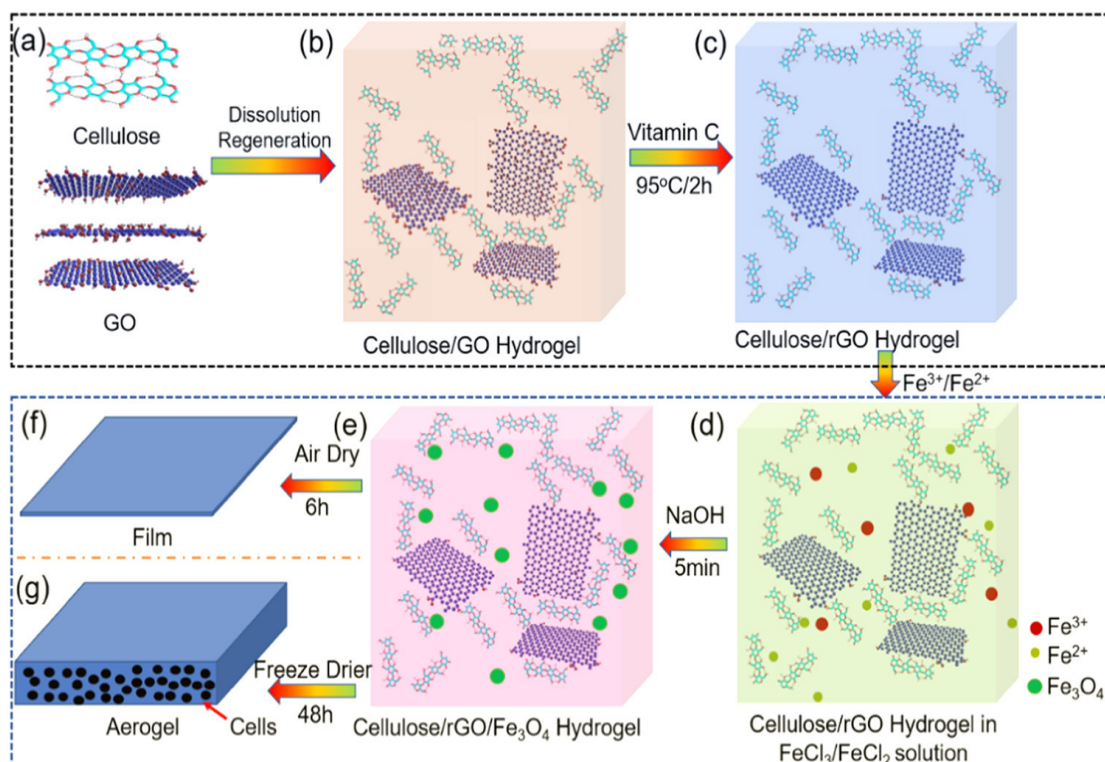
Figure 16. (**a**–**g**) Stepwise demonstration of the preparation of cellulose/rGO/Fe$_3$O$_4$ composite hydrogels, aerogels and films via freeze-drying and air-drying, respectively. Reproduced with permission from [156]. Copyright 2020, American Chemical Society.
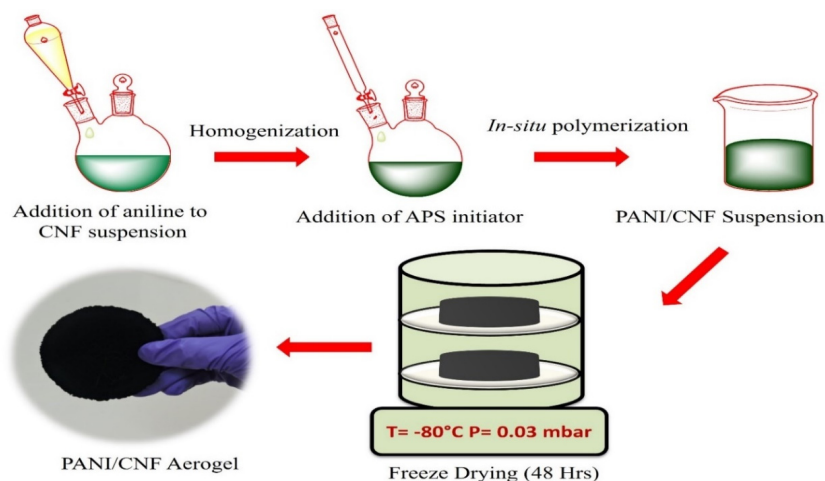

Figure 17. A demonstration of various steps involved in the fabrication of PANI/CNF aerogels. Reproduced with permission from [157]. Copyright 2020, Elsevier Ltd.

14. Intrinsically Conducting Polymer Aerogels for Electromagnetic Interference Shielding

Intrinsically conductive polymers (ICPs) refer to a group of organic polymers with unique electrical/optical properties that are similar to those of metals and inorganic semi-conductors. The key advantages of ICPs are that they can be easily synthesized in a simple and cost-effective manner using less expensive monomers via a simple electro-oxidative polymerization process. The quest for designing and synthesizing ICPs began in the mid-1950s, but garnered much more attention in the late 1970s thanks to the pioneering works of Alan J. Heeger, Alan MacDiarmid and Hideki Shirakawa, who later won the Nobel Prize in chemistry in the year 2000. Some of the well-known ICPs are polyacetylene (PA), polyaniline (PANi), poly[3,4-(ethylenedioxy)thiophene] (PEDOT), polythiophene (PT),

polypyrrole (PPy) and polyphenylene, which have been widely studied for various applications such as sensors, OLEDs, batteries, supercapacitors and EMI shielding [158,159]. In the past few decades, ICP aerogels have attracted a great deal of interest owing to their low density, high surface area and excellent electrical conductivity, especially for microwave-absorbing applications. In this view, Xie et al. [160] fabricated ultralight and 3D porous polypyrrole/nano-SiO$_2$ aerogels via an in situ gelation process, as shown in Figure 18a. Pyrrole monomer was dispersed along with nano-SiO$_2$ powder in H$_2$O/ethanol solution, followed by addition of anhydrous FeCl$_3$ to initiate polymerization. A dark-colored hydrogel was obtained, which was later dried under vacuum at 50 °C to form PPy/nano-SiO$_2$ aerogels. At 20% SiO$_2$ loading, the maximum effective electromagnetic absorption (EMA) bandwidth could reach 6.0 GHz at an absorber thickness of 2.5 mm [160]. It is envisaged that nano-SiO$_2$ was added to improve the impedance matching and improve the broadband EMA performance of the aerogels. In order to enhance the microwave absorption performance, magnetic materials can also be incorporated in ICP aerogels. In another study by Sui and coworkers, polydopamine-functionalized carbonyl iron powder-anchored polypyrrole (CIP@PPy) aerogels were examined for their microwave absorption ability. Herein, carbonyl iron powder was mechanically mixed along with a surfactant and dopamine hydrochloride to form polydopamine-coated carbonyl iron powder. This powder was later blended to a pyrrole monomer in H$_2$O/ethanol solution by ultra-sonication, and FeCl$_3$ was added dropwise to start polymerization, as shown in Figure 18b. This resulted in the formation of a black hydrogel, which was washed serval times with distilled water and ethanol to remove the unreacted monomers and impurities. The hydrogel was then then dried at 50 °C for 12 h to form CIP@PPy aerogels. These aerogels demonstrated two strong absorption peaks (min RL) of −38.9 and −39.5 dB at 12.2 and 14.2 GHz, respectively, at a 2.2 mm thickness [161]. It is also noteworthy that they showcased a broad bandwidth (min RL < −10 dB) of 6.1 GHz in the region of 10 to 16.1 GHz, which infers its commercial applicability in this frequency region. It is envisaged that this broad-bandwidth microwave absorption behavior is due to the presence of carbonyl iron powder in these aerogels
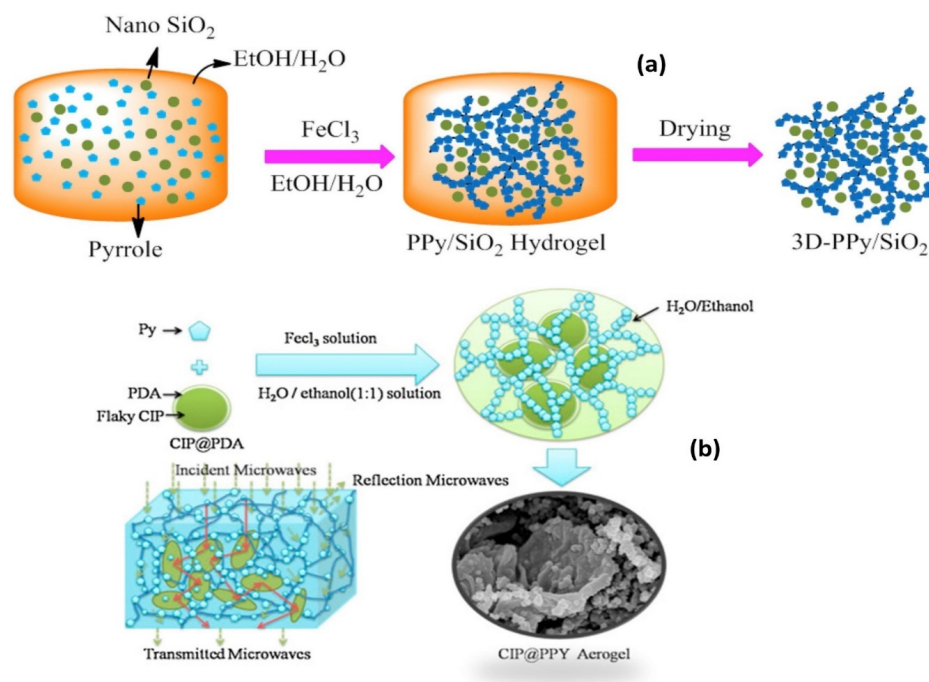

Figure 18. (**a**) The preparation of PPy/SiO$_2$ composites. (**b**) Schematic representation of the formation of CIP@PPy aerogels and the interaction of the microwave within the composite. Reproduced with permission from [160,161]. Copyright 2015, Elsevier Ltd.

15. Next-Generation 2D Materials for High-Performance Porous EMI Shields

Over the past decade, researchers have been actively working towards developing novel 2D materials with superior electronic, optical and mechanical properties when compared to existing 2D nanostructures such as graphene, boron nitride and metal dichalcogenides. Very recently, transition metal carbides, carbonitrides and nitrides, known as MXenes, are the latest additions to the world of 2D material. They were discovered by the pioneering works lead by Yury Gogotsi and Michel Barsoum from Drexel University, USA, in 2011 [162]. MXenes are synthesized by selective etching of certain atomic layers from their layered precursors, MAX phases, which are a family of ternary carbides and nitrides. MXenes have a general formula of $M_{n+1}X_nT_x$ ($n = 1$–3), where M corresponds to an early transition metal (such as Ti, Zr, Hf, Sc, V, Nb, Ta, Cr or Mo), X is C/N and T_x stands for the surface terminal groups such as hydroxyl, oxygen or fluorine. MXene showcases a high electrical conductivity of 1400 S.m^{-1} with a superior ability to form stable aqueous dispersions, good antibacterial properties and ease of processing. These unique properties makes MXene suitable for a wide range of applications, such as Li-ion, Li-S, Na-ion, Mg-ion batteries, supercapacitors, ultra-thin EMI shielding materials, water purification and biomedical applications. The high electrical conductivity of these 2D materials has encouraged researchers to fabricate porous architectures via suitable incorporation into a polymer matrix. In this view, Xu et al. [163] fabricated a series of lightweight, porous Ti_2CT_x MXene/poly(vinyl alcohol) (PVA) composite foams and flexible films via a simple freeze-drying technique and subsequent compressing of these foams, as shown in Figure 19a. Initially, few-layered Ti_2CT_x (f-Ti_2CT_x) was synthesized via a gentle etching of Ti_2AlC using LiF and HCl as etching agents. f-Ti_2CT_x was then mixed with PVA solutions at different concentrations to form stable hydrosols and subsequently freeze-dried for 48 h in a freeze-dryer at 0.1 Pa. These foams were then pressed under a rolling machine to form MXene/PVA films. The maximum EMI shielding values of these foams and films were 33 and 26 dB at 5 mm and ~100 μm, respectively. In the case of MXene/PVA foams, they exhibited a high specific shielding effectiveness of 5136 dB.cm^3.g^{-1} at an ultra-low MXene content of only 0.15 vol.%, with excellent absorption-dominated shielding performance [163]. Upon compression, these foams transform into flexible films that showcase enhanced conductivity (8.0×10^{-4} S/m), which could have resulted due to a decrease in porosity. The absorption- or reflection-dominant shielding behavior depends upon whether the incident EM wave can enter the shield material. In the case of MXene/PVA composite film, the incident EM wave is reflected back from the shield surface due to poor impedance matching, similar to metallic surfaces, whereas for the composite foam, a better impedance matching can be achieved which will minimize EM wave reflection. When the EM wave enters the bulk of foam, it will undergo multiple internal reflection within the porous network and the layered structure of the MXene flakes, which will end up as heat dissipation due to dipolar and interfacial polarization. The possible EMI shielding mechanism of MXene/PVA foam and film is demonstrated in Figure 19b.

In order to maintain the structural stability and induce the elastic property in MXene foams, Wu et al. [164] fabricated highly conductive polydimethylsiloxane (PDMS)-coated MXene foams. Initially, a 3D network of MXene/sodium alginate (SA) aerogel was fabricated by the directional freeze-drying process to form an anisotropic architecture, as shown in Figure 20. This was followed by coating the MXene/SA aerogel with a thin layer of PDMS by a vacuum-assisted process to form highly compressible MXene foams. These hybrid aerogels showcased an excellent conductivity of 2211 S.m^{-1} and a maximum EMI shielding value of 70.5 dB (more than 99.99999% incident EM energy is blocked). It is also noteworthy that the PDMS-coated MXene foam with 6.1 wt.% of MXene demonstrates high EMI shielding efficiency of 48.2 dB, even after 500 compression cycles [164]. Hence, PDMS-coated compressible and robust MXene foams demonstrate huge potential for EMI shielding applications for next-generation telecommunication, IoT systems, military and defense applications.
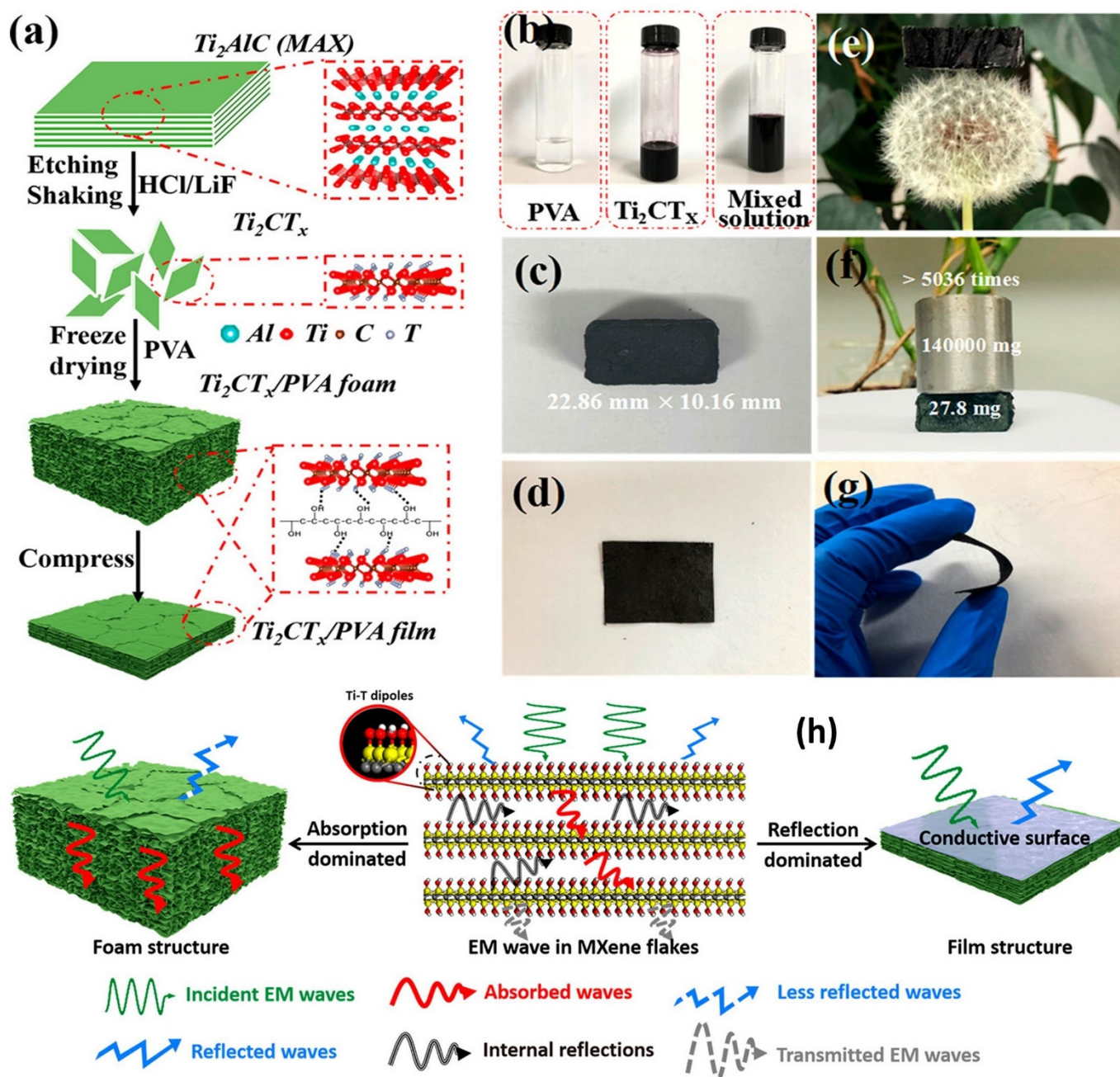
Figure 19. (**a**) Stepwise fabrication process of f-Ti$_2$CT$_x$/PVA composite film and foam. (**b**) Photographs of PVA solution (transparent), f-Ti$_2$CT$_x$ solution (black color) and f-Ti$_2$CT$_x$/PVA solution. (**c,d**) Images of f-Ti$_2$CT$_x$/PVA foam and film. (**e**) Piece of this foam on a dandelion, depicting its ultra-low density. (**f**) Photograph of this foam supporting more than 5000 times its own weight. (**g**) Flexibility of f-Ti$_2$CT$_x$/PVA film. (**h**) Plausible EMI shielding mechanism of foam- and film-based MXene/PVA composites. Reproduced with permission from [163]. Copyright 2019, American Chemical Society.
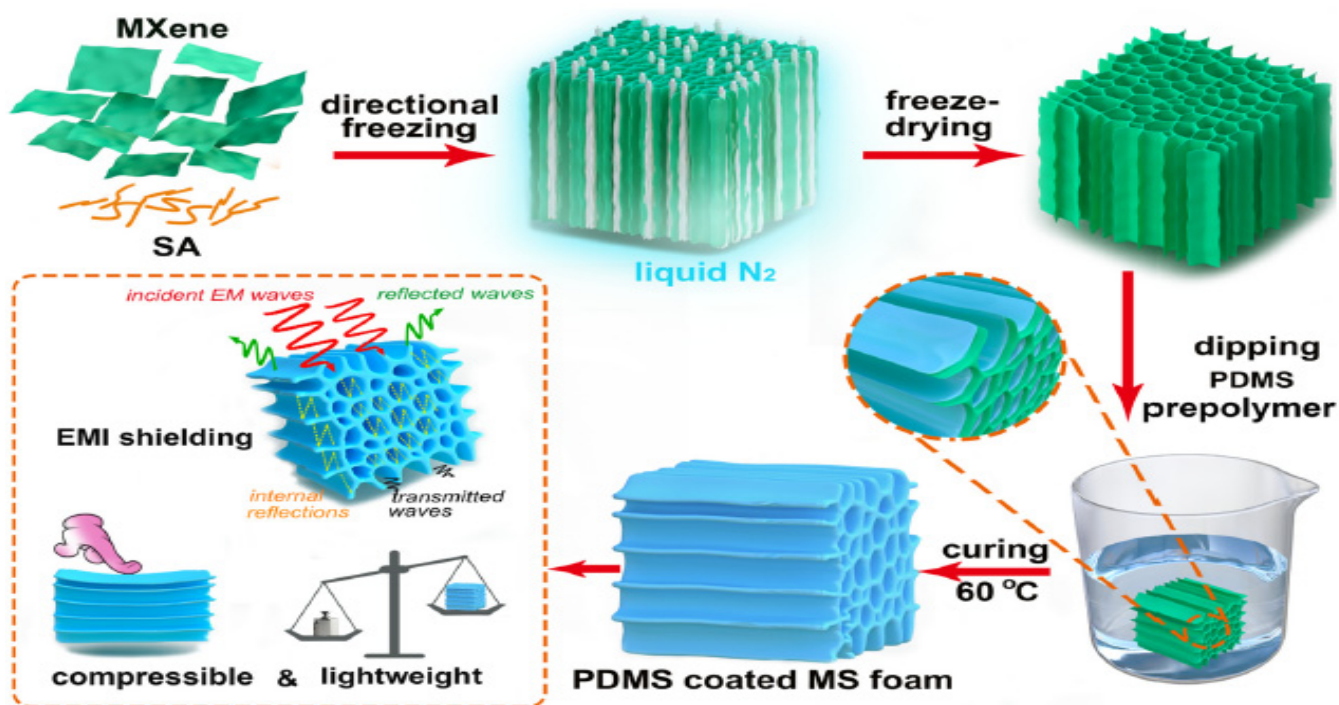
Figure 20. Schematic representing the fabrication of MXene/sodium alginate aerogel and its PDMS-coated foam. Reproduced with permission from [164]. Copyright 2020, Elsevier Ltd.

16. Conclusions and Future Outlook

This review encompasses various strategies adopted by researchers to fabricate porous polymer nanocomposites such as foams and aerogels to suppress electromagnetic interference via the microwave absorption phenomenon. The roles of nanostructured materials such as graphene, carbon nanotubes, MXenes and metal nanowires have been of paramount importance in EMI shielding applications, and the ability of these nanoinclusions to percolate within a polymeric system have inspired researchers to develop higher-performance EMI shielding materials. However, with the advancement of technology, the need for lightweight materials with superior EMI shielding performances has initiated burgeoning interest for porous materials for EMI shielding applications. Hence, designing engineered porous materials is considered as an effective strategy to reduce the overall density of the EMI shield as well as to reduce the percolation threshold of the system. It can also be observed that in all the porous engineered systems, the incoming electromagnetic radiation undergoes multiple internal reflections, and the reflected waves within the pores are eventually absorbed and dissipated as heat energy. Nevertheless, the mechanical properties of these aerogels and foams are also very crucial for their use in practical applications as microwave absorbers. Table 2 illustrated various aerogel/foam compositions reported in the literature for EMI shielding applications, with some key parameters depicting their shielding performance. In the near future, novel 2D materials such as MXene will play a key role in the development of self-assembled and engineered porous materials, which have the potential to deliver higher EMI shielding performances even at lower shielding thickness owing to their higher electrical conductivity and excellent physicochemical properties. The translation of these materials from the lab to industry is yet another hurdle that needs to be addressed in the near future. Hence, ultra-lightweight, robust and commercially viable porous architectures such as nanocomposite foams and aerogels are the most promising candidates for microwave absorption and suppressing electromagnetic pollution.

Abbreviations

1D	One-dimensional
2D	Two-dimensional
3D	Three-dimensional
AgNWs	Silver nanowires
$BaTiO_3$	Barium titanate
CB	Carbon Black
CFCs	Chlorofluorocarbons
CIP	Carbonyl iron powder
CO_2	Carbon dioxide
CNFs	Carbon nanofibers
CNTs	Carbon nanotubes
dB	Decibel
DC	Direct current
DCM	Dichloromethane
EAB	Electromagnetic absorption bandwidth
EM	Electromagnetic
EMI	Electromagnetic interference
EPLA	Expanded polylactic acid
$FeCl_3$	Ferric chloride
$FeCl_2$	Ferrous chloride
Fe_2O_3	Ferric oxide
Fe_3O_4	Iron oxide
GHz	Gigahertz
GO	Graphene oxide
GnP	Graphene nanoplatelet
hBN	Hexagonal boron nitride
HCl	Hydrochloric acid
HDPE	High-density polyethylene
Hz	Hertz
ICPs	Intrinsically conducting polymers
LiF	Lithium fluoride

MoS_2	Molybdenum disulfide
MG	Maxwell Garnett
MWCNTs	Multi-walled carbon nanotubes
NPs	Nanoparticles
NW	Nanowire
PA	Polyacetlyene
PAA	Polyamic acid
PANI	Polyaniline
$PbTiO_3$	Lead titanate
PDLA	Poly(D-lactide acid)
PDMS	Polydimethylsiloxane
PEDOT	Poly(3,4-rthylenedioxythiophene)
PEI	Polyethylenimine
PI	Polyimide
PLA	Polylactic acid
PLLA	Poly(L-lactide acid)
PP	Polypropylene
PPy	Polypyrrole
PS	Polystyrene
PSS	Polystyrene sulfonate
PT	Polythiophene
PU	Polyurathane
PUG	Polyurathene/graphene
PVA	Poly vinyl alcohol
R	Reflectivity
R_L	Reflection loss
rGO	Reduced graphene oxide
SA	Sodium alginate
ScPLA	Stereo complex polylactide
Sc-CO_2	Supercritical carbon dioxides
SE	Shielding effectiveness
SE_A	Shielding effectiveness due to absorption
SE_M	Shielding effectiveness due to multiple reflections
SE_R	Shielding effectiveness due to reflection
SEM	Scanning electron microscopy
SiO_2	Silicon dioxide
SSE	Specific shielding efficiency
SWCNTs	Single-walled carbon nanotubes
TEM	Transmission electron microscopy
TiO_2	Titanium dioxide
TPU	Thermoplastic polyurethanes
VMQ	Vinyl silicon rubber

References

1. *Health Effects of Exposure to EMF*; Scientific Committee on Emerging and Newly Identified Health Risks, European Commission: Brussels, Belgium, 2009.
2. Guidelines for Limiting Exposure to Electromagnetic Fields (100 kHz to 300 GHz), International Commission on Non-Ionizing Radiation Protection (ICNIRP). *Health Phys.* **2020**, *118*, 483–524. [CrossRef] [PubMed]
3. IEEE Standard for Safety Levels with Respect to Human Exposure to Electric, Magnetic, and Electromagnetic Fields, 0 Hz to 300 GHz. In *IEEE Std C95.1-2019 (Revision of IEEE Std C95.1-2005/Incorporates IEEE Std C95.1-2019/Cor 1-2019)*; IEEE Standard Association: Piscataway, NJ, USA, 2019; pp. 1–312. [CrossRef]
4. Tiikkaja, M.; Aro, A.L.; Alanko, T.; Lindholm, H.; Sistonen, H.; Hartikainen, J.E.; Toivonen, L.; Juutilainen, J.; Hietanen, M. Electromagnetic Interference with Cardiac Pacemakers and Implantable Cardioverter-Defibrillators from Low-Frequency Electromagnetic Fields in Vivo. *Europace* **2013**, *15*, 388–394. [CrossRef] [PubMed]
5. Liu, S.; Qin, S.; Jiang, Y.; Song, P.; Wang, H. Lightweight high-performance carbon-polymer nanocomposites for electromagnetic interference shielding. *Compos. Part A Appl. Sci. Manuf.* **2021**, *145*, 106376. [CrossRef]

6. Li, Y.; Sun, N.; Liu, J.; Hao, X.; Du, J.; Yang, H.; Li, X.; Cao, M. Multifunctional BiFeO$_3$ Composites: Absorption Attenuation Dominated Effective Electromagnetic Interference Shielding and Electromagnetic Absorption Induced by Multiple Dielectric and Magnetic Relaxations. *Compos. Sci. Technol.* **2018**, *159*, 240–250. [CrossRef]

7. Li, X.-H.; Li, X.; Liao, K.-N.; Min, P.; Liu, T.; Dasari, A.; Yu, Z.-Z. Thermally Annealed Anisotropic Graphene Aerogels and Their Electrically Conductive Epoxy Composites with Excellent Electromagnetic Interference Shielding Efficiencies. *ACS Appl. Mater. Interfaces* **2016**, *8*, 33230–33239. [CrossRef]

8. Zeng, Z.; Jin, H.; Chen, M.; Li, W.; Zhou, L.; Zhang, Z. Lightweight and Anisotropic Porous MWCNT/WPU Composites for Ultrahigh Performance Electromagnetic Interference Shielding. *Adv. Funct. Mater.* **2016**, *26*, 303–310. [CrossRef]

9. Wan, C.; Li, J. Synthesis and Electromagnetic Interference Shielding of Cellulose-Derived Carbon Aerogels Functionalized with α-Fe$_2$O$_3$ and Polypyrrole. *Carbohydr. Polym.* **2017**, *161*, 158–165. [CrossRef]

10. Wan, Y.-J.; Zhu, P.-L.; Yu, S.-H.; Sun, R.; Wong, C.-P.; Liao, W.-H. Ultralight, Super-Elastic and Volume-Preserving Cellulose Fiber/Graphene Aerogel for High-Performance Electromagnetic Interference Shielding. *Carbon* **2017**, *115*, 629–639. [CrossRef]

11. Huang, H.-D.; Liu, C.-Y.; Zhou, D.; Jiang, X.; Zhong, G.-J.; Yan, D.-X.; Li, Z.-M. Cellulose Composite Aerogel for Highly Efficient Electromagnetic Interference Shielding. *J. Mater. Chem. A* **2015**, *3*, 4983–4991. [CrossRef]

12. Guo, J.; Song, H.; Liu, H.; Luo, C.; Ren, Y.; Ding, T.; Khan, M.A.; Young, D.P.; Liu, X.; Zhang, X.; et al. Polypyrrole-Interface-Functionalized Nano-Magnetite Epoxy Nanocomposites as Electromagnetic Wave Absorbers with Enhanced Flame Retardancy. *J. Mater. Chem. C* **2017**, *5*, 5334–5344. [CrossRef]

13. Madani, M. Conducting Carbon Black Filled NR/ IIR Blend Vulcanizates: Assessment of the Dependence of Physical and Mechanical Properties and Electromagnetic Interference Shielding on Variation of Filler Loading. *J. Polym. Res.* **2010**, *17*, 53–62. [CrossRef]

14. Yang, W.; Shao, B.; Liu, T.; Zhang, Y.; Huang, R.; Chen, F.; Fu, Q. Robust and Mechanically and Electrically Self-Healing Hydrogel for Efficient Electromagnetic Interference Shielding. *ACS Appl. Mater. Interfaces* **2018**, *10*, 8245–8257. [CrossRef] [PubMed]

15. Zhao, B.; Zhao, C.; Hamidinejad, M.; Wang, C.; Li, R.; Wang, S.; Yasamin, K.; Park, C.B. Incorporating a Microcellular Structure into PVDF/Graphene-Nanoplatelet Composites to Tune Their Electrical Conductivity and Electromagnetic Interference Shielding Properties. *J. Mater. Chem. C* **2018**, *6*, 10292–10300. [CrossRef]

16. Zachariah, S.M.; Grohens, Y.; Kalarikkal, N.; Thomas, S. Hybrid Materials for Electromagnetic Shielding: A Review. *Polym. Compos.* **2022**, *43*, 2507–2544. [CrossRef]

17. Pawar, S.P.; Gandi, M.; Arief, I.; Krause, B.; Pötschke, P.; Bose, S. Graphene Derivatives Doped with Nickel Ferrite Nanoparticles as Excellent Microwave Absorbers in Soft Nanocomposites. *ChemistrySelect* **2017**, *2*, 5984–5999. [CrossRef]

18. Bora, P.J.; Mallik, N.; Ramamurthy, P.C.; Kishore, S.; Madras, G. Poly(Vinyl Butyral)-Polyaniline-Magnetically Functionalized Fly Ash Cenosphere Composite Film for Electromagnetic Interference Shielding. *Compos. Part B Eng.* **2016**, *106*, 224–233. [CrossRef]

19. Dalal, J.; Lather, S.; Gupta, A.; Tripathi, R.; Maan, A.S.; Singh, K.; Ohlan, A. Reduced Graphene Oxide Functionalized Strontium Ferrite in Poly(3,4-Ethylenedioxythiophene) Conducting Network: A High-Performance EMI Shielding Material. *Adv. Mater. Technol.* **2019**, *4*, 1900023. [CrossRef]

20. Hong, X.; Chung, D. Carbon Nanofiber Mats for Electromagnetic Interference Shielding. *Carbon* **2017**, *111*, 529–537. [CrossRef]

21. Yang, S.; Lozano, K.; Lomeli, A.; Foltz, H.D.; Jones, R. Electromagnetic Interference Shielding Effectiveness of Carbon Nanofiber/LCP Composites. *Compos. Part A Appl. Sci. Manuf.* **2005**, *36*, 691–697. [CrossRef]

22. Deeraj, B.; George, G.; Dhineshbabu, N.; Bose, S.; Joseph, K. Electrospun ZrO$_2$@carbon Nanofiber Mats and Their Epoxy Composites as Effective EMI Shields in Ku Band. *Mater. Res. Bull.* **2021**, *144*, 111477. [CrossRef]

23. Abraham, J.; Mohammed Arif, P.; Kailas, L.; Kalarikkal, N.; George, S.C.; Thomas, S. Developing Highly Conducting and Mechanically Durable Styrene Butadiene Rubber Composites with Tailored Microstructural Properties by a Green Approach Using Ionic Liquid Modified MWCNTs. *RSC Adv.* **2016**, *6*, 32493–32504. [CrossRef]

24. Kunjappan, A.M.; Poothanari, M.A.; Ramachandran, A.A.; Padmanabhan, M.; Mathew, L.; Thomas, S. High-Performance Electromagnetic Interference Shielding Material Based on an Effective Mixing Protocol. *Polym. Int.* **2019**, *68*, 637–647. [CrossRef]

25. Abraham, J.; Arif, P.M.; Xavier, P.; Bose, S.; George, S.C.; Kalarikkal, N.; Thomas, S. Investigation into Dielectric Behaviour and Electromagnetic Interference Shielding Effectiveness of Conducting Styrene Butadiene Rubber Composites Containing Ionic Liquid Modified MWCNT. *Polymer* **2017**, *112*, 102–115. [CrossRef]

26. Ajitha, A.A.; Mohammed Arif, M.P.; Aswathi, M.K.; Mathew, L.P.; Geethamma, G.; Kalarikkal, N.; Thomas, S.; Volova, T. An Effective EMI Shielding Material Based on Poly(Trimethylene Terephthalate) Blend Nanocomposites with Multiwalled Carbon Nanotubes. *New J. Chem.* **2018**, *42*, 13915–13926.

27. Poothanari, M.A.; Abraham, J.; Kalarikkal, N.; Thomas, S. Excellent Electromagnetic Interference Shielding and High Electrical Conductivity of Compatibilized Polycarbonate/Polypropylene Carbon Nanotube Blend Nanocomposites. *Ind. Eng. Chem. Res.* **2018**, *57*, 4287–4297. [CrossRef]

28. Sharika, T.; Abraham, J.; Arif, P.M.; George, S.C.; Kalarikkal, N.; Thomas, S. Excellent Electromagnetic Shield Derived from MWCNT Reinforced NR/PP Blend Nanocomposites with Tailored Microstructural Properties. *Compos. Part B Eng.* **2019**, *173*, 106798. [CrossRef]

29. Shin, B.; Mondal, S.; Lee, M.; Kim, S.; Huh, Y., II; Nah, C. Flexible Thermoplastic Polyurethane-Carbon Nanotube Composites for Electromagnetic Interference Shielding and Thermal Management. *Chem. Eng. J.* **2021**, *418*, 129282. [CrossRef]

30. Zhu, G.; Isaza, L.G.; Huang, B.; Dufresne, A. Multifunctional Nanocellulose/Carbon Nanotube Composite Aerogels for High-Efficiency Electromagnetic Interference Shielding. *ACS Sustain. Chem. Eng.* **2022**, *10*, 2397–2408. [CrossRef]

31. Sushmita, K.; Formanek, P.; Krause, B.; Pötschke, P.; Bose, S. Distribution of Carbon Nanotubes in Polycarbonate-Based Blends for Electromagnetic Interference Shielding. *ACS Appl. Nano Mater.* **2022**, *5*, 662–677. [CrossRef]

32. Lee, T.W.; Lee, S.E.; Jeong, Y.G. Highly Effective Electromagnetic Interference Shielding Materials Based on Silver Nanowire/Cellulose Papers. *ACS Appl. Mater. Interfaces* **2016**, *8*, 13123–13132. [CrossRef]

33. Ravindren, R.; Mondal, S.; Nath, K.; Das, N.C. Prediction of Electrical Conductivity, Double Percolation Limit and Electromagnetic Interference Shielding Effectiveness of Copper Nanowire Filled Flexible Polymer Blend Nanocomposites. *Compos. Part B Eng.* **2019**, *164*, 559–569. [CrossRef]

34. Ma, Z.; Xiang, X.; Shao, L.; Zhang, Y.; Gu, J. Multifunctional Wearable Silver Nanowire Decorated Leather Nanocomposites for Joule Heating, Electromagnetic Interference Shielding and Piezoresistive Sensing. *Angew. Chem. Int. Ed.* **2022**, *61*, e202200705. [CrossRef] [PubMed]

35. Xie, Q.; Yan, Z.; Wang, S.; Wang, Y.; Mei, L.; Qin, F.; Jiang, R. Transparent, Flexible, and Stable Polyethersulfone/Copper-Nanowires/Polyethylene Terephthalate Sandwich-Structured Films for High-Performance Electromagnetic Interference Shielding. *Adv. Eng. Mater.* **2021**, *23*, 2100283. [CrossRef]

36. Joshi, A.; Bajaj, A.; Singh, R.; Anand, A.; Alegaonkar, P.; Datar, S. Processing of Graphene Nanoribbon Based Hybrid Composite for Electromagnetic Shielding. *Compos. Part B Eng.* **2015**, *69*, 472–477. [CrossRef]

37. Zhang, H.-B.; Yan, Q.; Zheng, W.-G.; He, Z.; Yu, Z.-Z. Tough Graphene-Polymer Microcellular Foams for Electromagnetic Interference Shielding. *ACS Appl. Mater. Interfaces* **2011**, *3*, 918–924. [CrossRef]

38. Xu, J.; Li, R.; Ji, S.; Zhao, B.; Cui, T.; Tan, X.; Gou, G.; Jian, J.; Xu, H.; Qiao, Y.; et al. Multifunctional Graphene Microstructures Inspired by Honeycomb for Ultrahigh Performance Electromagnetic Interference Shielding and Wearable Applications. *ACS Nano* **2021**, *15*, 8907–8918. [CrossRef] [PubMed]

39. Tan, X.; Yuan, Q.; Qiu, M.; Yu, J.; Jiang, N.; Lin, C.-T.; Dai, W. Rational Design of Graphene/Polymer Composites with Excellent Electromagnetic Interference Shielding Effectiveness and High Thermal Conductivity: A Mini Review. *J. Mater. Sci. Technol.* **2022**, *117*, 238–250. [CrossRef]

40. Yan, D.-X.; Pang, H.; Li, B.; Vajtai, R.; Xu, L.; Ren, P.-G.; Wang, J.-H.; Li, Z.-M. Structured Reduced Graphene Oxide/Polymer Composites for Ultra-Efficient Electromagnetic Interference Shielding. *Adv. Funct. Mater.* **2015**, *25*, 559–566. [CrossRef]

41. Song, P.; Liang, C.; Wang, L.; Qiu, H.; Gu, H.; Kong, J.; Gu, J. Obviously Improved Electromagnetic Interference Shielding Performances for Epoxy Composites via Constructing Honeycomb Structural Reduced Graphene Oxide. *Compos. Sci. Technol.* **2019**, *181*, 107698. [CrossRef]

42. Li, J.; Zhao, X.; Wu, W.; Ji, X.; Lu, Y.; Zhang, L. Bubble-Templated RGO-Graphene Nanoplatelet Foams Encapsulated in Silicon Rubber for Electromagnetic Interference Shielding and High Thermal Conductivity. *Chem. Eng. J.* **2021**, *415*, 129054. [CrossRef]

43. Shen, Y.; Lin, Z.; Wei, J.; Xu, Y.; Wan, Y.; Zhao, T.; Zeng, X.; Hu, Y.; Sun, R. Facile Synthesis of Ultra-Lightweight Silver/Reduced Graphene Oxide (RGO) Coated Carbonized-Melamine Foams with High Electromagnetic Interference Shielding Effectiveness and High Absorption Coefficient. *Carbon* **2022**, *186*, 9–18. [CrossRef]

44. Sankaran, S.; Deshmukh, K.; Ahamed, M.B.; Sadasivuni, K.K.; Faisal, M.; Pasha, S.K. Electrical and Electromagnetic Interference (EMI) Shielding Properties of Hexagonal Boron Nitride Nanoparticles Reinforced Polyvinylidene Fluoride Nanocomposite Films. *Polym. Plast. Technol. Mater.* **2019**, *58*, 1191–1209. [CrossRef]

45. Zhan, Y.; Lago, E.; Santillo, C.; Del Río Castillo, A.E.; Hao, S.; Buonocore, G.G.; Chen, Z.; Xia, H.; Lavorgna, M.; Bonaccorso, F. An Anisotropic Layer-by-Layer Carbon Nanotube/Boron Nitride/Rubber Composite and Its Application in Electromagnetic Shielding. *Nanoscale* **2020**, *12*, 7782–7791. [CrossRef] [PubMed]

46. Habibi, N.; Pourjavadi, A. Superhydrophobic and Thermally Conductive Carbon Black/Hexagonal Boron Nitride@Fe$_3$O$_4$/Cellulose Composite Paper for Electromagnetic Interference Shielding. *Synth. Met.* **2022**, *285*, 117008. [CrossRef]

47. Shang, Y.; Ji, Y.; Dong, J.; Yang, G.; Zhang, X.; Su, F.; Feng, Y.; Liu, C. Sandwiched Cellulose Nanofiber/Boron Nitride Nanosheet/Ti3C2Tx MXene Composite Film with High Electromagnetic Shielding and Thermal Conductivity yet Insulation Performance. *Compos. Sci. Technol.* **2021**, *214*, 108974. [CrossRef]

48. Ding, X.; Huang, Y.; Li, S.; Zhang, N.; Wang, J. 3D Architecture Reduced Graphene Oxide-MoS$_2$ Composite: Preparation and Excellent Electromagnetic Wave Absorption Performance. *Compos. Part A Appl. Sci. Manuf.* **2016**, *90*, 424–432. [CrossRef]

49. Saboor, A.; Khalid, S.M.; Jan, R.; Khan, A.N.; Zia, T.; Farooq, M.U.; Afridi, S.; Sadiq, M.; Arif, M. PS/PANI/MoS$_2$ Hybrid Polymer Composites with High Dielectric Behavior and Electrical Conductivity for EMI Shielding Effectiveness. *Materials* **2019**, *12*, 2690. [CrossRef]

50. Prasad, J.; Singh, A.K.; Tomar, M.; Gupta, V.; Singh, K. Hydrothermal Synthesis of Micro-Flower like Morphology Aluminum-Doped MoS$_2$/RGO Nanohybrids for High Efficient Electromagnetic Wave Shielding Materials. *Ceram. Int.* **2021**, *47*, 15648–15660. [CrossRef]

51. Prasad, J.; Singh, A.K.; Singh Gahlot, A.P.; Tomar, M.; Gupta, V.; Singh, K. Electromagnetic Interference Shielding Properties of Hierarchical Core-Shell Palladium-Doped MoS$_2$/CNT Nanohybrid Materials. *Ceram. Int.* **2021**, *47*, 27586–27597. [CrossRef]

52. Liu, R.; Miao, M.; Li, Y.; Zhang, J.; Cao, S.; Feng, X. Ultrathin Biomimetic Polymeric Ti$_3$C$_2$T$_x$ MXene Composite Films for Electromagnetic Interference Shielding. *ACS Appl. Mater. Interfaces* **2018**, *10*, 44787–44795. [CrossRef]

53. Wan, Y.-J.; Li, X.-M.; Zhu, P.-L.; Sun, R.; Wong, C.-P.; Liao, W.-H. Lightweight, Flexible MXene/Polymer Film with Simultaneously Excellent Mechanical Property and High-Performance Electromagnetic Interference Shielding. *Compos. Part A Appl. Sci. Manuf.* **2020**, *130*, 105764. [CrossRef]

54. Zeng, Z.H.; Wu, N.; Wei, J.J.; Yang, Y.F.; Wu, T.T.; Li, B.; Hauser, S.B.; Yang, W.D.; Liu, J.R.; Zhao, S.Y. Porous and Ultra-Flexible Crosslinked MXene/Polyimide Composites for Multifunctional Electromagnetic Interference Shielding. *Nano Micro Lett.* **2022**, *14*, 59. [CrossRef] [PubMed]

55. Liu, J.; Mckeon, L.; Garcia, J.; Pinilla, S.; Barwich, S.; Möbius, M.; Stamenov, P.; Coleman, J.N.; Nicolosi, V. Additive Manufacturing of Ti3C2-MXene-Functionalized Conductive Polymer Hydrogels for Electromagnetic-Interference Shielding. *Adv. Mater.* **2022**, *34*, 2106253. [CrossRef] [PubMed]

56. Zhu, Y.; Liu, J.; Guo, T.; Wang, J.J.; Tang, X.; Nicolosi, V. Multifunctional $Ti_3C_2T_x$ MXene Composite Hydrogels with Strain Sensitivity toward Absorption-Dominated Electromagnetic-Interference Shielding. *ACS Nano* **2021**, *15*, 1465–1474. [CrossRef] [PubMed]

57. Hong, S.Y.; Kim, Y.C.; Wang, M.; Nam, J.D.; Suhr, J. Anisotropic Electromagnetic Interference Shielding Properties of Polymer-Based Composites with Magnetically-Responsive Aligned Fe_3O_4 Decorated Reduced Graphene Oxide. *Eur. Polym. J.* **2020**, *127*, 109595. [CrossRef]

58. Li, Y.; Xue, B.; Yang, S.; Cheng, Z.; Xie, L.; Zheng, Q. Flexible Multilayered Films Consisting of Alternating Nanofibrillated Cellulose/Fe_3O_4 and Carbon Nanotube/Polyethylene Oxide Layers for Electromagnetic Interference Shielding. *Chem. Eng. J.* **2021**, *410*, 128356. [CrossRef]

59. Zhang, Y.; Ma, Z.; Ruan, K.; Gu, J. Multifunctional $Ti_3C_2T_x$-(Fe_3O_4/Polyimide) Composite Films with Janus Structure for Outstanding Electromagnetic Interference Shielding and Superior Visual Thermal Management. *Nano Res.* **2022**, 1–9. [CrossRef]

60. Singh, A.P.; Garg, P.; Alam, F.; Singh, K.; Mathur, R.B.; Tandon, R.P.; Chandra, A.; Dhawan, S.K. Phenolic Resin-Based Composite Sheets Filled with Mixtures of Reduced Graphene Oxide, γ-Fe_2O_3 and Carbon Fibers for Excellent Electromagnetic Interference Shielding in the X-Band. *Carbon* **2012**, *50*, 3868–3875. [CrossRef]

61. Chen, K.Y.; Gupta, S.; Tai, N.H. Reduced Graphene Oxide/Fe_2O_3 Hollow Microspheres Coated Sponges for Flexible Electromagnetic Interference Shielding Composites. *Compos. Commun.* **2021**, *23*, 100572. [CrossRef]

62. Wang, Y.; Wang, W.; Qi, Q.; Xu, N.; Yu, D. Layer-by-Layer Assembly of PDMS-Coated Nickel Ferrite/Multiwalled Carbon Nanotubes/Cotton Fabrics for Robust and Durable Electromagnetic Interference Shielding. *Cellulose* **2020**, *27*, 2829–2845. [CrossRef]

63. Wang, Y.; Qi, Q.; Yin, G.; Wang, W.; Yu, D. Flexible, Ultralight, and Mechanically Robust Waterborne Polyurethane/$Ti_3C_2T_X$ MXene/Nickel Ferrite Hybrid Aerogels for High-Performance Electromagnetic Interference Shielding. *ACS Appl. Mater. Interfaces* **2021**, *13*, 21831–21843. [CrossRef] [PubMed]

64. Saini, P.; Arora, M.; Gupta, G.; Gupta, B.K.; Singh, V.N.; Choudhary, V. High Permittivity Polyaniline–Barium Titanate Nanocomposites with Excellent Electromagnetic Interference Shielding Response. *Nanoscale* **2013**, *5*, 4330–4336. [CrossRef] [PubMed]

65. Sambyal, P.; Singh, A.P.; Verma, M.; Farukh, M.; Singh, B.P.; Dhawan, S.K. Tailored Polyaniline/Barium Strontium Titanate/Expanded Graphite Multiphase Composite for Efficient Radar Absorption. *RSC Adv.* **2014**, *4*, 12614–12624. [CrossRef]

66. Joseph, J.; Deshmukh, K.; Raj, A.N.; Pasha, S.K.K. Electromagnetic Interference Shielding Characteristics of $SrTiO_3$ Nanoparticles Induced Polyvinyl Chloride and Polyvinylidene Fluoride Blend Nanocomposites. *J. Inorg. Organomet. Polym. Mater.* **2021**, *31*, 3481–3495. [CrossRef]

67. Mohanapriya, M.K.; Deshmukh, K.; Kadlec, J.; Sadasivuni, K.K.; Faisal, M.; Nambi Raj, N.A.; Pasha, S.K.K. Dynamic Mechanical Analysis and Broadband Electromagnetic Interference Shielding Characteristics of Poly (Vinyl Alcohol)-Poly (4-Styrenesulfonic Acid)-Titanium Dioxide Nanoparticles Based Tertiary Nanocomposites. *Polym. Technol. Mater.* **2020**, *59*, 847–863. [CrossRef]

68. Tong, X.; Li, W.; Li, J.; Lu, S.; Wang, B.; Ma, K.; Yang, C.; Li, Q. In Situ Generation of TiO_2 in Graphene Aerogel and Its Epoxy Composite for Electromagnetic Interference Shielding Performance. *J. Mater. Sci. Mater. Electron.* **2022**, *33*, 5886–5898. [CrossRef]

69. Gopakumar, D.A.; Pai, A.R.; Pottathara, Y.B.; Pasquini, D.; De Morais, L.C.; Luke, M.; Kalarikkal, N.; Grohens, Y.; Thomas, S. Cellulose Nanofiber-Based Polyaniline Flexible Papers as Sustainable Microwave Absorbers in the X-Band. *ACS Appl. Mater. Interfaces* **2018**, *10*, 20032–20043. [CrossRef]

70. Zhang, Y.; Pan, T.; Yang, Z. Flexible Polyethylene Terephthalate/Polyaniline Composite Paper with Bending Durability and Effective Electromagnetic Shielding Performance. *Chem. Eng. J.* **2020**, *389*, 124433. [CrossRef]

71. Li, J.; Li, Y.; Yang, L.; Yin, S. Ti3C2Tx/PANI/Liquid Metal Composite Microspheres with 3D Nanoflower Structure: Preparation, Characterization, and Applications in EMI Shielding. *Adv. Mater. Interfaces* **2022**, *9*, 2102266. [CrossRef]

72. Maruthi, N.; Faisal, M.; Raghavendra, N.; Prasanna, B.; Manohara, S.; Revanasiddappa, M. Promising EMI Shielding Effectiveness and Anticorrosive Properties of PANI-Nb2O5 Nanocomposites: Multifunctional Approach. *Synth. Met.* **2021**, *275*, 116744. [CrossRef]

73. Gopakumar, D.A.; Pai, A.R.; Pottathara, Y.B.; Pasquini, D.; de Morais, L.C.; Khalil, H.P.S.A.; Nzihou, A.; Thomas, S. Flexible Papers Derived from Polypyrrole Deposited Cellulose Nanofibers for Enhanced Electromagnetic Interference Shielding in Gigahertz Frequencies. *J. Appl. Polym. Sci.* **2021**, *138*, 50262. [CrossRef]

74. Parit, M.; Du, H.; Zhang, X.; Prather, C.; Adams, M.; Jiang, Z. Polypyrrole and Cellulose Nanofiber Based Composite Films with Improved Physical and Electrical Properties for Electromagnetic Shielding Applications. *Carbohydr. Polym.* **2020**, *240*, 116304. [CrossRef] [PubMed]

75. Pasha, A.; Khasim, S.; Darwish, A.; Hamdalla, T.A.; Al-Ghamdi, S.; Alfadhli, S. Flexible, Stretchable and Electrically Conductive PDMS Decorated with Polypyrrole/Manganese-Iron Oxide Nanocomposite as a Multifunctional Material for High Performance EMI Shielding Applications. *Synth. Met.* **2022**, *283*, 116984. [CrossRef]

76. Dai, Y.-L.; Zhang, X.-J.; Wen, B.-Y.; Du, Q.-Y. Facile Synthesis of Polypyrrole Nanoparticles with Tunable Conductivity for Efficient Electromagnetic Wave Absorption and Shielding Performance. *CrystEngComm* **2022**, *24*, 3287–3296. [CrossRef]

77. Bora, P.J.; Anil, A.G.; Vinoy, K.J.; Ramamurthy, P.C. Outstanding Absolute Electromagnetic Interference Shielding Effectiveness of Cross-Linked PEDOT:PSS Film. *Adv. Mater. Interfaces* **2019**, *6*, 1901353. [CrossRef]

78. Al-Asbahi, B.A.; Qaid, S.M.; El-Shamy, A.G. Flexible Conductive Nanocomposite PEDOT:PSS/Te Nanorod Films for Superior Electromagnetic Interference (EMI) Shielding: A New Exploration. *J. Ind. Eng. Chem.* **2021**, *100*, 233–247. [CrossRef]

79. Das, P.; Ganguly, S.; Perelshtein, I.; Margel, S.; Gedanken, A. Acoustic Green Synthesis of Graphene-Gallium Nanoparticles and PEDOT:PSS Hybrid Coating for Textile To Mitigate Electromagnetic Radiation Pollution. *ACS Appl. Nano Mater.* **2022**, *5*, 1644–1655. [CrossRef]

80. Iqbal, S.; Shah, J.; Kotnala, R.K.; Ahmad, S. Highly Efficient Low Cost EMI Shielding by Barium Ferrite Encapsulated Polythiophene Nanocomposite. *J. Alloys Compd.* **2019**, *779*, 487–496. [CrossRef]

81. Iqbal, S.; Khatoon, H.; Kotnala, R.K.; Ahmad, S. Electromagnetic Interference Shielding Performance by Thermally Stable Magnesium Ferrite Encapsulated Polythiophene Composite. *J. Mater. Sci. Mater. Electron.* **2021**, *32*, 19191–19202. [CrossRef]

82. Alamri, S.; Rajhi, A.A.; Anqi, A.E.; Tran, N. Enhanced Microwave Dissipation Features of $BiFe_{0.8}Co_{0.1}Mn_{0.1}O_3/MWCNTs$ Composite Decorate of Polythiophene. *J. Magn. Magn. Mater.* **2022**, *545*, 168724. [CrossRef]

83. Chung, D.D.L. Materials for Electromagnetic Interference Shielding. *J. Mater. Eng. Perform.* **2000**, *9*, 350–354. [CrossRef]

84. Li, R.; Ding, L.; Gao, Q.; Zhang, H.; Zeng, D.; Zhao, B.; Fan, B.; Zhang, R. Tuning of anisotropic electrical conductivity and enhancement of EMI shielding of polymer composite foam via CO_2-assisted delamination and orientation of MXene. *Chem. Eng. J.* **2021**, *415*, 128930. [CrossRef]

85. Gupta, P.; Singh, B.; Agrawal, A.; Maji, P.K. Low Density and High Strength Nanofibrillated Cellulose Aerogel for Thermal Insulation Application. *Mater. Des.* **2018**, *158*, 224–236. [CrossRef]

86. Zhang, Z.; Tan, J.; Gu, W.; Zhao, H.; Zheng, J.; Zhang, B.; Ji, G. Cellulose-Chitosan Framework/Polyailine Hybrid Aerogel toward Thermal Insulation and Microwave Absorbing Application. *Chem. Eng. J.* **2020**, *395*, 125190. [CrossRef]

87. Mi, H.Y.; Jing, X.; Politowicz, A.L.; Chen, E.; Huang, H.X.; Turng, L.S. Highly Compressible Ultra-Light Anisotropic Cellulose/Graphene Aerogel Fabricated by Bidirectional Freeze Drying for Selective Oil Absorption. *Carbon* **2018**, *132*, 199–209. [CrossRef]

88. Yao, Y.; Jin, S.; Zou, H.; Li, L.; Ma, X.; Lv, G.; Gao, F.; Lv, X.; Shu, Q. Polymer-Based Lightweight Materials for Electromagnetic Interference Shielding: A Review. *J. Mater. Sci.* **2021**, *56*, 6549–6580. [CrossRef]

89. Saini, P.; Choudhary, V.; Singh, B.P.; Mathur, R.B.; Dhawan, S.K. Enhanced Microwave Absorption Behavior of Polyaniline-CNT/Polystyrene Blend in 12.4–18.0 GHz Range. *Synth. Met.* **2011**, *161*, 1522–1526. [CrossRef]

90. Shahzad, F.; Alhabeb, M.; Hatter, C.B.; Anasori, B.; Hong, S.M.; Koo, C.M.; Gogotsi, Y. Electromagnetic Interference Shielding with 2D Transition Metal Carbides (MXenes). *Science* **2016**, *353*, 1137–1140. [CrossRef]

91. Weng, L.; Lei, X.; Liu, J.; Hu, H.; Wang, J.; Zhang, Z. Three-dimensional network FeNi/C composites with excellent microwave-absorbing properties. *J. Alloys Compd.* **2022**, *906*, 164301. [CrossRef]

92. Mohammed, J.; Tchouank Tekou Carol, T.; Hafeez, H.Y.; Basandrai, D.; Bhadu, G.R.; Godara, S.K.; Narang, S.B.; Srivastava, A.K. Electromagnetic Interference (EMI)Shielding, Microwave Absorption, and Optical Sensing Properties of BaM/CCTO Composites in K_u-Band. *Results Phys.* **2019**, *13*, 102307. [CrossRef]

93. Dhakate, S.R.; Subhedar, K.M.; Singh, B.P. Polymer Nanocomposite Foam Filled with Carbon Nanomaterials as an Efficient Electromagnetic Interference Shielding Material. *RSC Adv.* **2015**, *5*, 43036–43057. [CrossRef]

94. Zhang, Y.; Cai, R.; Wang, D.; Li, K.; Sun, Q.; Xiao, Y.; Teng, H.; Huang, X.; Sun, T.; Liu, Z.; et al. Lightweight, Low-Cost Co_2SiO_4@diatomite Core-Shell Composite Material for High-Efficiency Microwave Absorption. *Molecules* **2022**, *27*, 1055. [CrossRef] [PubMed]

95. Ling, J.; Zhai, W.; Feng, W.; Shen, B.; Zhang, J.; Zheng, W.G. Facile Preparation of Lightweight Microcellular Polyetherimide/Graphene Composite Foams for Electromagnetic Interference Shielding. *ACS Appl. Mater. Interfaces* **2013**, *5*, 2677–2684. [CrossRef] [PubMed]

96. Cheng, Y.; Cao, J.; Li, Y.; Li, Z.; Zhao, H.; Ji, G.; Du, Y. The Outside-In Approach to Construct Fe_3O_4 Nanocrystals/Mesoporous Carbon Hollow Spheres Core–Shell Hybrids toward Microwave Absorption. *ACS Sustain. Chem. Eng.* **2018**, *6*, 1427–1435. [CrossRef]

97. Yan, J.; Huang, Y.; Liu, X.; Zhao, X.; Li, T.; Zhao, Y.; Liu, P. Polypyrrole-Based Composite Materials for Electromagnetic Wave Absorption. *Polym. Rev.* **2021**, *61*, 646–687. [CrossRef]

98. Shukla, V. Review of Electromagnetic Interference Shielding Materials Fabricated by Iron Ingredients. *Nanoscale Adv.* **2019**, *1*, 1640–1671. [CrossRef]

99. Hamidinejad, M.; Zhao, B.; Zandieh, A.; Moghimian, N.; Filleter, T.; Park, C.B. Enhanced Electrical and Electromagnetic Interference Shielding Properties of Polymer-Graphene Nanoplatelet Composites Fabricated via Supercritical-Fluid Treatment and Physical Foaming. *ACS Appl. Mater. Interfaces* **2018**, *10*, 30752–30761. [CrossRef]

100. Peng, M.; Qin, F. Clarification of basic concepts for electromagnetic interference shielding effectiveness. *J. Appl. Phys.* **2021**, *130*, 225108. [CrossRef]

101. Jia, L.-C.; Yan, D.-X.; Cui, C.-H.; Jiang, X.; Ji, X.; Li, Z.-M. Electrically Conductive and Electromagnetic Interference Shielding of Polyethylene Composites with Devisable Carbon Nanotube Networks. *J. Mater. Chem. C* **2015**, *3*, 9369–9378. [CrossRef]

102. Jin, F.-L.; Zhao, M.; Park, M.; Park, S.-J. Recent Trends of Foaming in Polymer Processing: A Review. *Polymers* **2019**, *11*, 953. [CrossRef]

103. Sauceau, M.; Fages, J.; Common, A.; Nikitine, C.; Rodier, E. New Challenges in Polymer Foaming: A Review of Extrusion Processes Assisted by Supercritical Carbon Dioxide. *Prog. Polym. Sci.* **2011**, *36*, 749–766. [CrossRef]

104. Lavoine, N.; Bergström, L. Nanocellulose-Based Foams and Aerogels: Processing, Properties, and Applications. *J. Mater. Chem. A* **2017**, *5*, 16105–16117. [CrossRef]

105. Budtova, T. Cellulose II Aerogels: A Review. *Cellulose* **2019**, *26*, 81–121. [CrossRef]

106. Yang, J.; Liao, X.; Li, J.; He, G.; Zhang, Y.; Tang, W.; Wang, G.; Li, G. Light-Weight and Flexible Silicone Rubber/MWCNTs/Fe_3O_4 Nanocomposite Foams for Efficient Electromagnetic Interference Shielding and Microwave Absorption. *Compos. Sci. Technol.* **2019**, *181*, 107670. [CrossRef]

107. Li, Y.; Li, C.; Zhao, S.; Cui, J.; Zhang, G.; Gao, A.; Yan, Y. Facile Fabrication of Highly Conductive and Robust Three-Dimensional Graphene/Silver Nanowires Bicontinuous Skeletons for Electromagnetic Interference Shielding Silicone Rubber Nanocomposites. *Compos. Part A Appl. Sci. Manuf.* **2019**, *119*, 101–110. [CrossRef]

108. Zhao, S.; Yan, Y.; Gao, A.; Zhao, S.; Cui, J.; Zhang, G. Flexible Polydimethylsilane Nanocomposites Enhanced with a Three-Dimensional Graphene/Carbon Nanotube Bicontinuous Framework for High-Performance Electromagnetic Interference Shielding. *ACS Appl. Mater. Interfaces* **2018**, *10*, 26723–26732. [CrossRef]

109. Chen, J.; Liao, X.; Xiao, W.; Yang, J.; Jiang, Q.; Li, G. Facile and Green Method to Structure Ultralow-Threshold and Lightweight Polystyrene/MWCNT Composites with Segregated Conductive Networks for Efficient Electromagnetic Interference Shielding. *ACS Sustain. Chem. Eng.* **2019**, *7*, 9904–9915. [CrossRef]

110. Ju, J.; Kuang, T.; Ke, X.; Zeng, M.; Chen, Z.; Zhang, S.; Peng, X. Lightweight Multifunctional Polypropylene/Carbon Nanotubes/Carbon Black Nanocomposite Foams with Segregated Structure, Ultralow Percolation Threshold and Enhanced Electromagnetic Interference Shielding Performance. *Compos. Sci. Technol.* **2020**, *193*, 108116. [CrossRef]

111. Li, Y.; Shen, B.; Yi, D.; Zhang, L.; Zhai, W.; Wei, X.; Zheng, W. The Influence of Gradient and Sandwich Configurations on the Electromagnetic Interference Shielding Performance of Multilayered Thermoplastic Polyurethane/Graphene Composite Foams. *Compos. Sci. Technol.* **2017**, *138*, 209–216. [CrossRef]

112. Jiang, Q.; Liao, X.; Li, J.; Chen, J.; Wang, G.; Yi, J.; Yang, Q.; Li, G. Flexible Thermoplastic Polyurethane/Reduced Graphene Oxide Composite Foams for Electromagnetic Interference Shielding with High Absorption Characteristic. *Compos. Part A Appl. Sci. Manuf.* **2019**, *123*, 310–319. [CrossRef]

113. Shen, B.; Li, Y.; Zhai, W.; Zheng, W. Compressible Graphene-Coated Polymer Foams with Ultralow Density for Adjustable Electromagnetic Interference (EMI) Shielding. *ACS Appl. Mater. Interfaces* **2016**, *8*, 8050–8057. [CrossRef] [PubMed]

114. Wang, G.; Wang, L.; Mark, L.H.; Shaayegan, V.; Wang, G.; Li, H.; Zhao, G.; Park, C.B. Ultralow-Threshold and Lightweight Biodegradable Porous PLA/MWCNT with Segregated Conductive Networks for High-Performance Thermal Insulation and Electromagnetic Interference Shielding Applications. *ACS Appl. Mater. Interfaces* **2018**, *10*, 1195–1203. [CrossRef] [PubMed]

115. Cui, C.-H.; Yan, D.-X.; Pang, H.; Jia, L.-C.; Xu, X.; Yang, S.; Xu, J.-Z.; Li, Z.-M. A High Heat-Resistance Bioplastic Foam with Efficient Electromagnetic Interference Shielding. *Chem. Eng. J.* **2017**, *323*, 29–36. [CrossRef]

116. Wang, Y.Y.; Zhou, Z.H.; Zhou, C.G.; Sun, W.J.; Gao, J.F.; Dai, K.; Yan, D.X.; Li, Z.M. Lightweight and Robust Carbon Nanotube/Polyimide Foam for Efficient and Heat-Resistant Electromagnetic Interference Shielding and Microwave Absorption. *ACS Appl. Mater. Interfaces* **2020**, *12*, 8704–8712. [CrossRef] [PubMed]

117. Li, J.; Ding, Y.; Yu, N.; Gao, Q.; Fan, X.; Wei, X.; Zhang, G.; Ma, Z.; He, X. Lightweight and Stiff Carbon Foams Derived from Rigid Thermosetting Polyimide Foam with Superior Electromagnetic Interference Shielding Performance. *Carbon* **2020**, *158*, 45–54. [CrossRef]

118. Lu, D.; Mo, Z.; Liang, B.; Yang, L.; He, Z.; Zhu, H.; Tang, Z.; Gui, X. Flexible, lightweight carbon nanotube sponges and composites for high-performance electromagnetic interference shielding. *Carbon* **2018**, *133*, 457–463. [CrossRef]

119. Yousefi, N.; Sun, X.; Lin, X.; Shen, X.; Jia, J.; Zhang, B.; Tang, B.; Chan, M.; Kim, J.-K. Highly Aligned Graphene/Polymer Nanocomposites with Excellent Dielectric Properties for High-Performance Electromagnetic Interference Shielding. *Adv. Mater.* **2014**, *26*, 5480–5487. [CrossRef]

120. Shen, B.; Zhai, W.; Tao, M.; Ling, J.; Zheng, W. Lightweight, Multifunctional Polyetherimide/Graphene@Fe_3O_4 Composite Foams for Shielding of Electromagnetic Pollution. *ACS Appl. Mater. Interfaces* **2013**, *5*, 11383–11391. [CrossRef]

121. Xi, J.; Li, Y.; Zhou, E.; Liu, Y.; Gao, W.; Guo, Y.; Ying, J.; Chen, Z.; Chen, G.; Gao, C. Graphene aerogel films with expansion enhancement effect of high-performance electromagnetic interference shielding. *Carbon* **2018**, *135*, 44–51. [CrossRef]

122. Bi, S.; Zhang, L.; Mu, C.; Liu, M.; Hu, X. Applied Surface Science Electromagnetic Interference Shielding Properties and Mechanisms of Chemically Reduced Graphene Aerogels. *Appl. Surf. Sci.* **2017**, *412*, 529–536. [CrossRef]

123. Wang, L.; Liu, M.; Wang, G.; Dai, B.; Yu, F.; Zhang, J. An ultralight nitrogen-doped carbon aerogel anchored by Ni-NiO nanoparticles for enhanced microwave adsorption performance. *J. Alloys Compd.* **2018**, *776*, 43–51. [CrossRef]

124. Wang, H.; Meng, F.; Li, J.; Li, T.; Chen, Z.; Luo, H.; Zhou, Z. Carbonized Design of Hierarchical Porous Carbon/Fe$_3$O$_4$@Fe Derived from Loofah Sponge to Achieve Tunable High-Performance Microwave Absorption. *ACS Sustain. Chem. Eng.* **2018**, *6*, 11801–11810. [CrossRef]

125. Crespo, M.; González, M.; Elías, A.L.; Rajukumar, L.P.; Baselga, J.; Terrones, M.; Pozuelo, J. Ultra-Light Carbon Nanotube Sponge as an Efficient Electromagnetic Shielding Material in the GHz Range. *Phys. Status Solidi Rapid Res. Lett.* **2014**, *8*, 698–704. [CrossRef]

126. Chen, Y.; Zhang, H.-B.; Yang, Y.; Wang, M.; Cao, A.; Yu, Z.-Z. High-Performance Epoxy Nanocomposites Reinforced with Three-Dimensional Carbon Nanotube Sponge for Electromagnetic Interference Shielding. *Adv. Funct. Mater.* **2016**, *26*, 447–455. [CrossRef]

127. Zeng, Z.; Wang, C.; Zhang, Y.; Wang, P.; Shahabadi, S.I.S.; Pei, Y.; Chen, M.; Lu, X. Ultralight and Highly Elastic Graphene/Lignin-Derived Carbon Nanocomposite Aerogels with Ultrahigh Electromagnetic Interference Shielding Performance. *ACS Appl. Mater. Interfaces* **2018**, *10*, 8205–8213. [CrossRef] [PubMed]

128. Wang, C.; Ding, Y.; Yuan, Y.; He, X.; Wu, S.; Hu, S.; Zou, M.; Zhao, W.; Yang, L.; Cao, A.; et al. Graphene aerogel composites derived from recycled cigarette filters for electromagnetic wave absorption. *J. Mater. Chem. C* **2015**, *3*, 11893–11901. [CrossRef]

129. Song, W.; Guan, X.-T.; Fan, L.-Z.; Cao, W.-Q.; Wang, C.-Y.; Cao, M.-S. Tuning Three-Dimensional Textures with Graphene Aerogels for Ultra-Light Flexible Graphene/Texture Composites of Effective Electromagnetic Shielding. *Carbon* **2015**, *93*, 151–160. [CrossRef]

130. Ren, F.; Guo, Z.; Shi, Y.; Jia, L.; Qing, Y.; Ren, P.; Yan, D. Lightweight and Highly Efficient Electromagnetic Wave-Absorbing of 3D CNTs/GNS@CoFe$_2$O$_4$ Ternary Composite Aerogels. *J. Alloys Compd.* **2018**, *768*, 6–14. [CrossRef]

131. Chen, Y.; Zhang, H.-B.; Wang, M.; Qian, X.; Dasari, A.; Yu, Z.-Z. Phenolic Resin-Enhanced Three-Dimensional Graphene Aerogels and Their Epoxy Nanocomposites with High Mechanical and Electromagnetic Interference Shielding Performances. *Compos. Sci. Technol.* **2017**, *152*, 254–262. [CrossRef]

132. Li, X.; Yin, X.; Song, C.; Han, M.; Xu, H.; Duan, W.; Cheng, L.; Zhang, L. Self-Assembly Core–Shell Graphene-Bridged Hollow MXenes Spheres 3D Foam with Ultrahigh Specific EM Absorption Performance. *Adv. Funct. Mater.* **2018**, *28*, 1803938. [CrossRef]

133. Bian, R.; He, G.; Zhi, W.; Xiang, S.; Wang, T.; Cai, D. Ultralight MXene-Based Aerogels with High Electromagnetic Interference Shielding Performance. *J. Mater. Chem. C* **2019**, *7*, 474–478. [CrossRef]

134. Liu, J.; Zhang, H.-B.; Sun, R.; Liu, Y.; Liu, Z.; Zhou, A.; Yu, Z.-Z. Hydrophobic, Flexible, and Lightweight MXene Foams for High-Performance Electromagnetic-Interference Shielding. *Adv. Mater.* **2017**, *29*, 1702367. [CrossRef] [PubMed]

135. Chen, Z.; Xu, C.; Ma, C.; Ren, W.; Cheng, H.-M. Lightweight and Flexible Graphene Foam Composites for High-Performance Electromagnetic Interference Shielding. *Adv. Mater.* **2013**, *25*, 1296–1300. [CrossRef] [PubMed]

136. Wan, C.; Li, J. Graphene Oxide/Cellulose Aerogels Nanocomposite: Preparation, Pyrolysis, and Application for Electromagnetic Interference Shielding. *Carbohydr. Polym.* **2016**, *150*, 172–179. [CrossRef]

137. Ameli, A.; Jung, P.U.; Park, C.B. Electrical Properties and Electromagnetic Interference Shielding Effectiveness of Polypropylene/Carbon Fiber Composite Foams. *Carbon* **2013**, *60*, 379–391. [CrossRef]

138. Yan, D.-X.; Ren, P.-G.; Pang, H.; Fu, Q.; Yang, M.-B.; Li, Z.-M. Efficient Electromagnetic Interference Shielding of Lightweight Graphene/Polystyrene Composite. *J. Mater. Chem.* **2012**, *22*, 18772–18774. [CrossRef]

139. Ameli, A.; Nofar, M.; Wang, S.; Park, C.B. Lightweight Polypropylene/Stainless-Steel Fiber Composite Foams with Low Percolation for Efficient Electromagnetic Interference Shielding. *ACS Appl. Mater. Interfaces* **2014**, *6*, 11091–11100. [CrossRef] [PubMed]

140. Ma, J.; Zhan, M.; Wang, K. Ultralightweight Silver Nanowires Hybrid Polyimide Composite Foams for High-Performance Electromagnetic Interference Shielding. *ACS Appl. Mater. Interfaces* **2015**, *7*, 563–576. [CrossRef] [PubMed]

141. Li, Y.; Pei, X.; Shen, B.; Zhai, W.; Zhang, L.; Zheng, W. Polyimide/Graphene Composite Foam Sheets with Ultrahigh Thermostability for Electromagnetic Interference Shielding. *RSC Adv.* **2015**, *5*, 24342–24351. [CrossRef]

142. Wu, Y.; Wang, Z.; Liu, X.; Shen, X.; Zheng, Q.; Xue, Q.; Kim, J.-K. Ultralight Graphene Foam/Conductive Polymer Composites for Exceptional Electromagnetic Interference Shielding. *ACS Appl. Mater. Interfaces* **2017**, *9*, 9059–9069. [CrossRef]

143. Hsiao, S.T.; Ma, C.C.M.; Liao, W.H.; Wang, Y.S.; Li, S.M.; Huang, Y.C.; Yang, R.B.; Liang, W.F. Lightweight and Flexible Reduced Graphene Oxide/Water-Borne Polyurethane Composites with High Electrical Conductivity and Excellent Electromagnetic Interference Shielding Performance. *ACS Appl. Mater. Interfaces* **2014**, *6*, 10667–10678. [CrossRef] [PubMed]

144. Gavgani, J.N.; Adelnia, H.; Zaarei, D.; Moazzami Gudarzi, M. Lightweight Flexible Polyurethane/Reduced Ultralarge Graphene Oxide Composite Foams for Electromagnetic Interference Shielding. *RSC Adv.* **2016**, *6*, 27517–27527. [CrossRef]

145. Fletcher, A.; Gupta, M.C.; Dudley, K.L.; Vedeler, E. Elastomer Foam Nanocomposites for Electromagnetic Dissipation and Shielding Applications. *Compos. Sci. Technol.* **2010**, *70*, 953–958. [CrossRef]

146. Wu, F.; Xie, A.; Sun, M.; Wang, Y.; Wang, M. Reduced Graphene Oxide (RGO) Modified Spongelike Polypyrrole (PPy) Aerogel for Excellent Electromagnetic Absorption. *J. Mater. Chem. A* **2015**, *3*, 14358–14369. [CrossRef]

147. Zhan, Y.; Wang, J.; Zhang, K.; Li, Y.; Meng, Y.; Yan, N.; Wei, W.; Peng, F.; Xia, H. Fabrication of a Flexible Electromagnetic Interference Shielding Fe$_3$O$_4$@reduced Graphene Oxide/Natural Rubber Composite with Segregated Network. *Chem. Eng. J.* **2018**, *344*, 184–193. [CrossRef]

148. Zhao, W.; Shao, G.; Jiang, M.; Zhao, B.; Wang, H.; Chen, D.; Xu, H.; Li, X.; Zhang, R.; An, L. Ultralight Polymer-Derived Ceramic Aerogels with Wide Bandwidth and Effective Electromagnetic Absorption Properties. *J. Eur. Ceram. Soc.* **2017**, *37*, 3973–3980. [CrossRef]

149. Li, C.; Yang, G.; Deng, H.; Wang, K.; Zhang, Q.; Chen, F.; Fu, Q. The Preparation and Properties of Polystyrene/Functionalized Graphene Nanocomposite Foams Using Supercritical Carbon Dioxide. *Polym. Int.* **2013**, *62*, 1077–1084. [CrossRef]

150. Gedler, G.; Antunes, M.; Velasco, J.I.; Ozisik, R. Electromagnetic Shielding Effectiveness of Polycarbonate/Graphene Nanocomposite Foams Processed in 2-Steps with Supercritical Carbon Dioxide. *Mater. Lett.* **2015**, *160*, 41–44. [CrossRef]

151. Li, J.; Zhang, G.; Zhang, H.; Fan, X.; Zhou, L.; Shang, Z.; Shi, X. Electrical Conductivity and Electromagnetic Interference Shielding of Epoxy Nanocomposite Foams Containing Functionalized Multi-Wall Carbon Nanotubes. *Appl. Surf. Sci.* **2018**, *428*, 7–16. [CrossRef]

152. Tran, M.-P.; Thomassin, J.-M.; Alexandre, M.; Jérôme, C.; Huynen, I.; Detrembleur, C. Nanocomposite Foams of Polypropylene and Carbon Nanotubes: Preparation, Characterization, and Evaluation of Their Performance as EMI Absorbers. *Macromol. Chem. Phys.* **2015**, *216*, 1302–1312. [CrossRef]

153. Verma, M.; Chauhan, S.S.; Dhawan, S.K.; Choudhary, V. Graphene Nanoplatelets/Carbon Nanotubes/Polyurethane Composites as Efficient Shield against Electromagnetic Polluting Radiations. *Compos. Part B Eng.* **2017**, *120*, 118–127. [CrossRef]

154. Pai, A.R.; Paoloni, C.; Thomas, S. Nanocellulose-Based Sustainable Microwave Absorbers to Stifle Electromagnetic Pollution. In *Nanocellulose Based Composites for Electronics*; Elsevier: Amsterdam, The Netherlands, 2021; pp. 237–258. ISBN 9780128223505.

155. Zeng, Z.; Wu, T.; Han, D.; Ren, Q.; Siqueira, G.; Nyström, G. Ultralight, Flexible, and Biomimetic Nanocellulose/Silver Nanowire Aerogels for Electromagnetic Interference Shielding. *ACS Nano* **2020**, *14*, 2927–2938. [CrossRef] [PubMed]

156. Chen, Y.; Pötschke, P.; Pionteck, J.; Voit, B.; Qi, H. Multifunctional Cellulose/RGO/Fe$_3$O$_4$ Composite Aerogels for Electromagnetic Interference Shielding. *ACS Appl. Mater. Interfaces* **2020**, *12*, 22088–22098. [CrossRef]

157. Pai, A.R.; Binumol, T.; Gopakumar, D.A.; Pasquini, D.; Seantier, B.; Kalarikkal, N.; Thomas, S. Ultra-Fast Heat Dissipating Aerogels Derived from Polyaniline Anchored Cellulose Nanofibers as Sustainable Microwave Absorbers. *Carbohydr. Polym.* **2020**, *246*, 116663. [CrossRef] [PubMed]

158. Pai, A.R.; Nair, G.G.; Thomas, P.C.; Thomas, S. High-Performance Conducting Polymer Nanocomposites for EMI Shielding Applications. In *Conducting Polymers for Advanced Energy Applications*; CRC Press: Boca Raton, FL, USA, 2021; pp. 383–398.

159. Pai, A.R.; Thomas, S.; Kalarikkal, N. Electromagnetic Interference Shielding Composition, Article and Methods Thereof 2021. Available online: https://patentimages.storage.googleapis.com/4b/11/5b/7c0d91c5f85814/WO2021094836A1.pdf (accessed on 27 March 2022).

160. Xie, A.; Wu, F.; Xu, Z.; Wang, M. In Situ Preparation of Ultralight Three-Dimensional Polypyrrole/Nano SiO$_2$ Composite Aerogels with Enhanced Electromagnetic Absorption. *Compos. Sci. Technol.* **2015**, *117*, 32–38. [CrossRef]

161. Sui, M.; Lü, X.; Xie, A.; Xu, W.; Rong, X.; Wu, G. The Synthesis of Three-Dimensional (3D) Polydopamine-Functioned Carbonyl Iron Powder@polypyrrole (CIP@PPy) Aerogel Composites for Excellent Microwave Absorption. *Synth. Met.* **2015**, *210*, 156–164. [CrossRef]

162. Naguib, M.; Kurtoglu, M.; Presser, V.; Lu, J.; Niu, J.; Heon, M.; Hultman, L.; Gogotsi, Y.; Barsoum, M.W. Two-Dimensional Nanocrystals: Two-Dimensional Nanocrystals Produced by Exfoliation of Ti3AlC2 (Adv. Mater. 37/2011). *Adv. Mater.* **2011**, *23*, 4207. [CrossRef]

163. Xu, H.; Yin, X.; Li, X.; Li, M.; Liang, S.; Zhang, L.; Cheng, L. Lightweight Ti$_2$CT$_x$ MXene/Poly(Vinyl Alcohol) Composite Foams for Electromagnetic Wave Shielding with Absorption-Dominated Feature. *ACS Appl. Mater. Interfaces* **2019**, *11*, 10198–10207. [CrossRef]

164. Wu, X.; Han, B.; Zhang, H.-B.; Xie, X.; Tu, T.; Zhang, Y.; Dai, Y.; Yang, R.; Yu, Z.-Z. Compressible, Durable and Conductive Polydimethylsiloxane-Coated MXene Foams for High-Performance Electromagnetic Interference Shielding. *Chem. Eng. J.* **2020**, *381*, 122622. [CrossRef]